Cell

Selective Inhibition of Tumor Oncogenes by Disruption of Super-Enhancers

Jakob Lovén,[1,7] Heather A. Hoke,[1,2,7] Charles Y. Lin,[1,3,5,7] Ashley Lau,[1,2] David A. Orlando,[1] Christopher R. Vakoc,[4] James E. Bradner,[5,6] Tong Ihn Lee,[1] and Richard A. Young[1,2,*]
[1]Whitehead Institute for Biomedical Research, 9 Cambridge Center, Cambridge, MA 02142, USA
[2]Department of Biology
[3]Computational and Systems Biology Program
Massachusetts Institute of Technology, Cambridge, MA 02139, USA
[4]Cold Spring Harbor Laboratory, 1 Bungtown Road, Cold Spring Harbor, NY 11724, USA
[5]Department of Medical Oncology, Dana-Farber Cancer Institute, 44 Binney Street, Boston, MA 02115, USA
[6]Department of Medicine, Harvard Medical School, 25 Shattuck Street, Boston, MA 02115, USA
[7]These authors contributed equally to this work
*Correspondence: young@wi.mit.edu
http://dx.doi.org/10.1016/j.cell.2013.03.036

SUMMARY

Chromatin regulators have become attractive targets for cancer therapy, but it is unclear why inhibition of these ubiquitous regulators should have gene-specific effects in tumor cells. Here, we investigate how inhibition of the widely expressed transcriptional coactivator BRD4 leads to selective inhibition of the *MYC* oncogene in multiple myeloma (MM). BRD4 and Mediator were found to co-occupy thousands of enhancers associated with active genes. They also co-occupied a small set of exceptionally large super-enhancers associated with genes that feature prominently in MM biology, including the *MYC* oncogene. Treatment of MM tumor cells with the BET-bromodomain inhibitor JQ1 led to preferential loss of BRD4 at super-enhancers and consequent transcription elongation defects that preferentially impacted genes with super-enhancers, including *MYC*. Super-enhancers were found at key oncogenic drivers in many other tumor cells. These observations have implications for the discovery of cancer therapeutics directed at components of super-enhancers in diverse tumor types.

INTRODUCTION

Chromatin regulators are attractive as therapeutic targets for cancer because they are deregulated in numerous cancers (Baylin and Jones, 2011; Elsässer et al., 2011; Esteller, 2008; Feinberg and Tycko, 2004; You and Jones, 2012) and are amenable to small-molecule inhibition (Cole, 2008; Dawson and Kouzarides, 2012; Geutjes et al., 2012). Inhibition of some chromatin regulators has already proven to be efficacious for treatment of certain cancers (Issa and Kantarjian, 2009; Marks and Xu, 2009). Most chromatin regulators, however, are expressed in a broad range of healthy cells and contribute generally to gene expression, so inhibition of these important genome-associated proteins might be expected to adversely affect global gene expression in healthy cells and thus produce highly toxic effects. Nonetheless, inhibitors of some chromatin regulators, such as BRD4, have been shown to selectively inhibit transcription of key oncogenic drivers such as *c-MYC* (hereafter referred to as *MYC*) in multiple tumor types (Dawson et al., 2011; Delmore et al., 2011; Mertz et al., 2011; Zuber et al., 2011). It is important to understand how inhibition of a widely expressed, general regulator such as BRD4 can exert a selective effect on the expression of a small number of genes in specific cells.

BRD4 is a member of the bromodomain and extraterminal (BET) subfamily of human bromodomain proteins, which includes BRDT, BRD2, BRD3, and BRD4. These proteins associate with acetylated chromatin and facilitate transcriptional activation (LeRoy et al., 2008; Rahman et al., 2011). BRD4 was first identified as an interaction partner of the murine Mediator coactivator complex (Jiang et al., 1998) and was subsequently shown to associate with Mediator in a variety of human cells (Dawson et al., 2011; Wu and Chiang, 2007). BRD4 is involved in the control of transcriptional elongation by RNA polymerase II (RNA Pol II) through its recruitment of the positive transcription elongation factor P-TEFb (Jang et al., 2005; Yang et al., 2005). Almost all human cells express the *BRD4* gene, based on analysis of human tissue expression data across 90 distinct tissue types (human body index - transcriptional profiling, see Extended Experimental Procedures), and BRD4 is found to be associated with a large population of active genes in $CD4^+$ T cells (Zhang et al., 2012). It is not yet clear whether the BRD4 protein is generally involved in the transcription of active genes in tumor cells or if it is selectively associated with a subset of these genes.

Two recently developed bromodomain inhibitors, JQ1 and iBET, selectively bind to the amino-terminal twin bromodomains of BRD4 (Filippakopoulos et al., 2010; Nicodeme et al., 2010). These BET inhibitors cause selective repression of the potent *MYC* oncogene in a range of tumors, including multiple myeloma (MM), Burkitt's lymphoma (BL), acute myeloid leukemia (AML), and acute lymphoblastic leukemia (ALL) (Dawson et al., 2011; Delmore et al., 2011; Mertz et al., 2011; Ott et al., 2012; Zuber et al., 2011). The inhibition of *MYC* apparently occurs as a consequence of BRD4 depletion at the enhancers that drive *MYC* expression (Delmore et al., 2011). Although BRD4 is widely expressed in mouse tissues, mice are reasonably tolerant of the levels of BET bromodomain inhibition that inhibit certain tumors in mouse models (Dawson et al., 2011; Delmore et al., 2011; Filippakopoulos et al., 2010; Mertz et al., 2011; Zuber et al., 2011).

The MM cell line (MM1.S) used to study the effects of JQ1 has an *IgH-MYC* rearrangement, and *MYC* gene expression is driven by factors associated with the *IgH* enhancer (Dib et al., 2008; Shou et al., 2000). Enhancers function through cooperative and synergistic interactions between multiple transcription factors and coactivators (Carey et al., 1990; Giese et al., 1995; Kim and Maniatis, 1997; Thanos and Maniatis, 1995). Cooperative binding and synergistic activation confer increased sensitivity so that small changes in activator concentration can lead to dramatic changes in activator binding and transcription of associated genes (Carey, 1998). Furthermore, enhancers with large numbers of transcription factor binding sites can be more sensitive to small changes in factor concentration than those with smaller numbers of binding sites (Giniger and Ptashne, 1988; Griggs and Johnston, 1991). This concept led us to postulate that some features of the *IgH* enhancer might account for the selective effect of BRD4 inhibition.

We show here that BRD4 and Mediator are associated with most active enhancers and promoters in MM1.S tumor cells, but exceptionally high levels of these cofactors occur at a small set of large enhancer regions, which we call super-enhancers. Super-enhancers are associated with *MYC* and other key genes that feature prominently in the biology of MM, including many lineage-specific survival genes. Treatment of MM tumor cells with the BRD4 inhibitor JQ1 caused a preferential loss of BRD4, Mediator, and P-TEFb at super-enhancers and caused preferential loss of transcription at super-enhancer-associated genes, including the *MYC* oncogene. Tumor cell addiction to high-level expression of these oncogenes may then contribute to their vulnerability to super-enhancer disruption (Chin et al., 1999; Felsher and Bishop, 1999; Jain et al., 2002; Weinstein, 2002). We find super-enhancers in additional tumor types, where they are similarly associated with key oncogenes. Thus, key oncogene drivers of tumor cells are regulated by super-enhancers, which can confer disproportionate sensitivity to loss of the BRD4 coactivator and thus cause selective inhibition of transcription.

RESULTS

BRD4 and Mediator Co-occupy Promoters of Active Genes in Multiple Myeloma

Transcription factors bind to enhancers and recruit the Mediator coactivator, which in turn becomes associated with RNA Pol II at the transcription start site (TSS), thus forming DNA loops between enhancers and core promoters (Kagey et al., 2010). BRD4 is known to associate with Mediator in some mammalian cells (Dawson et al., 2011; Jiang et al., 1998; Wu et al., 2003). To identify active promoter and enhancer elements and to determine how BRD4 and Mediator occupy the genome in MM1.S MM cells, we used chromatin immunoprecipitation coupled to high-throughput sequencing (chromatin immunoprecipitation [ChIP]-seq) with antibodies against the Mediator subunit MED1, BRD4, the enhancer-associated histone modification H3K27Ac, and the TSS-associated histone modification H3K4Me3 (Figure 1). ChIP-seq signals for both Mediator and the histone modification H3K27Ac have previously been shown to occur at both enhancers and TSSs (Creyghton et al., 2010; Heintzman et al., 2009; Rada-Iglesias et al., 2011), and enhancers can be distinguished from TSSs by the absence of TSS annotation and relatively low levels of H3K4Me3. We found that BRD4 co-occupied enhancers and TSSs with MED1 throughout the genome (Figures 1A and 1B) and that the levels of BRD4 and MED1 were strongly correlated (Figure S1 available online).

To confirm that BRD4 and Mediator are generally associated with active genes in MM1.S cells, we compared the ChIP-seq data for these regulators with that for RNA Pol II and the histone modification H3K4Me3. The levels of BRD4 and Mediator correlated with the levels of RNA Pol II genome wide (Figure 1C). Signals for BRD4 and Mediator were found together with those for the histone modification H3K4Me3 and RNA Pol II at ~10,000 annotated TSSs, and these were considered active TSSs (Table S1). Signals for BRD4 and the enhancer-associated histone modification H3K27Ac were found in ~8,000 Mediator-occupied regions either lacking TSSs or extending beyond the immediate vicinity of the TSS, and these were considered enhancer regions (Table S2, Data S1, and Extended Experimental Procedures).

Super-Enhancers Are Associated with Key Multiple Myeloma Genes

Further analysis of the ~8,000 enhancer regions revealed that the MED1 signal at 308 enhancers was significantly greater than at all other enhancers and promoters (Figures 2A and S2A and Table S2). These 308 super-enhancers differed from typical enhancers in both size and Mediator levels (Figure 2B). Remarkably, ~40% of all enhancer-bound Mediator and BRD4 occupied these 308 super-enhancers. Whereas the typical enhancer had a median size of 1.3 kb, the super-enhancers had a median size of 19.4 kb. These super-enhancers were thus 15-fold larger than typical enhancers and were occupied, based on ChIP-seq signal, by 18-fold more Mediator and 16-fold more BRD4. Similarly high levels of H3K27Ac were observed in these large regions (Figure 2B). Examples of gene tracks showing super-enhancers at either end of the spectrum of Mediator occupancy (Figure 2A) are shown in Figure 2C. The largest super-enhancer was found associated with the *IGLL5* gene, which encodes an immunoglobulin lambda peptide expressed at high levels in these cells.

We next sought to identify the complete set of MM1.S genes that are most likely associated with super-enhancers. Enhancers tend to loop to and associate with adjacent genes in order to activate their transcription (Göndör and Ohlsson, 2009; Lelli

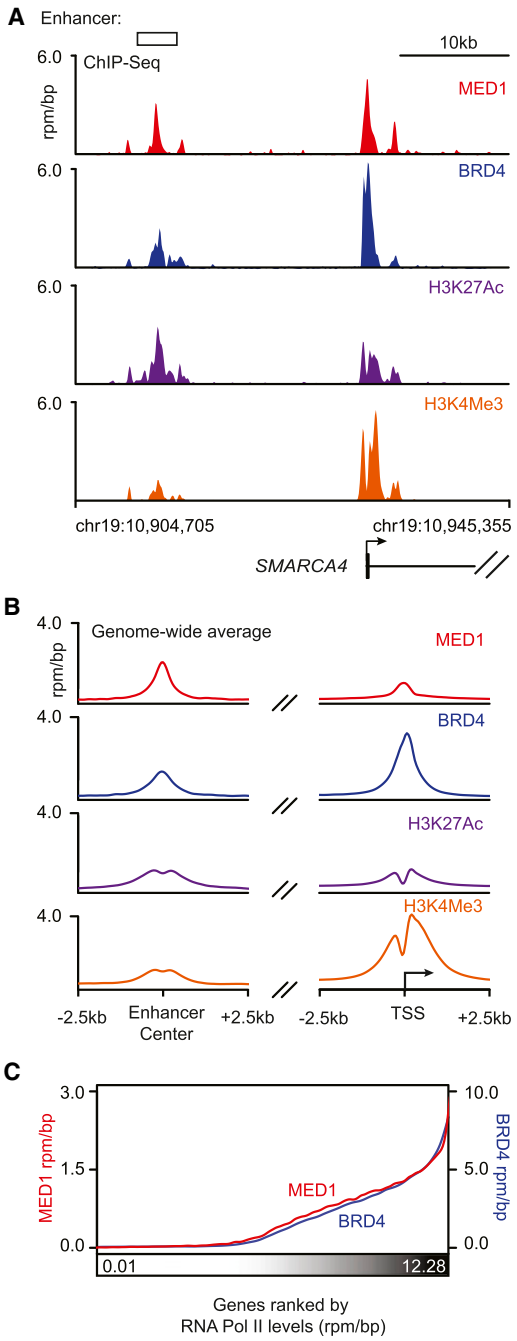

Figure 1. Mediator and BRD4 Co-occupy Promoters of Active Genes in Multiple Myeloma

(A) Gene tracks of MED1, BRD4, H3K27Ac, and H3K4Me3 ChIP-seq occupancy at the enhancer (left) and promoter (right) of *SMARCA4* in MM1.S MM cells. The x axis shows genomic position, and enhancer-containing regions are depicted with a white box. The y axis shows signal of ChIP-seq occupancy in units of reads per million mapped reads per base pair (rpm/bp).

(B) Metagene representation of global MED1, BRD4, H3K27Ac, and H3K4Me3 occupancy at enhancers and promoters. The x axis shows the ±2.5 kb region flanking either the center of enhancer regions (left) or the TSS of active genes (right). The y axis shows the average background subtracted ChIP-seq signal in units of rpm/bp.

(C) Median MED1 and BRD4 levels in the ±1 kb region around the TSSs of actively transcribed genes ranked by increasing RNA Pol II occupancy in MM1.S cells. Levels are in units of rpm/bp, with the left y axis showing levels of MED1 and the right y axis showing levels of BRD4. Promoters were binned (50/bin), and a smoothing function was applied to median levels.

See also Figure S1.

et al., 2012; Ong and Corces, 2011; Spitz and Furlong, 2012). Most of these interactions occur within a distance of ~50 kb of the enhancer (Chepelev et al., 2012). Using a simple proximity rule, we assigned all transcriptionally active genes (TSSs) to super-enhancers within a 50 kb window, a method shown to identify a large proportion of true enhancer/promoter interactions in embryonic stem cells (Dixon et al., 2012). This identified 681 genes associated with super-enhancers (Table S3), and 307 of these had a super-enhancer overlapping a portion of the gene, as shown for *CCND2* in Figure 2C.

Super-enhancer-associated genes were generally expressed at higher levels than genes with typical enhancers and tended to be specifically expressed in MM1.S cells (Figure 2D). To test whether components of super-enhancers confer stronger activity compared to typical enhancers, we cloned representative super-enhancer or typical enhancer fragments of similar size into luciferase reporter constructs and transfected these into MM1.S cells. Cloned sequence fragments from super-enhancers generated 2- to 3-fold higher luciferase activity compared to typical enhancers of similar size (Figure 2E and Extended Experimental Procedures). These results are consistent with the notion that super-enhancers help to activate high levels of transcription of key genes that regulate and enforce the MM1.S cancer cell state.

The super-enhancer-associated genes included most genes that have previously been shown to have important roles in MM biology, including *MYC*, *IRF4*, *PRDM1/BLIMP-1*, and *XBP1* (Figure 3A). *MYC* is a key oncogenic driver in MM (Chng et al., 2011; Dib et al., 2008; Holien et al., 2012; Shou et al., 2000), and the MM1.S *MYC* locus contains a chromosomal rearrangement that places *MYC* under the control of the *IgH* enhancer, which qualifies as a super-enhancer in MM1.S cells. The *IRF4* gene encodes a key plasma cell transcription factor that is frequently deregulated in MM (Shaffer et al., 2008). *PRDM1/BLIMP-1* encodes a transcription factor that is considered a master regulator of plasma cell development and is required for the formation of plasma cell tumors in a mouse model (Shapiro-Shelef et al., 2003; Turner et al., 1994). *XBP1* encodes a basic-region leucine zipper (bZIP) transcription factor of the CREB-ATF family that governs plasma cell differentiation (Reimold et al., 2001). *XBP1* is frequently overexpressed in human MM and can drive the development of MM in a mouse model (Carrasco et al., 2007; Claudio et al., 2002).

Super-enhancers were associated with many additional genes that have important roles in cancer pathogenesis more generally (Figure 3B). Cyclin D2 (*CCND2*) is deregulated in many human cancers, including MM (Bergsagel et al., 2005; Musgrove et al., 2011). The PIM1 kinase has been implicated in the biology of many different cancers (Shah et al., 2008). *MCL1* and *BCL-xL*, members of the BCL-2 family of apoptosis regulators, are frequently deregulated in cancer, promoting cell survival and

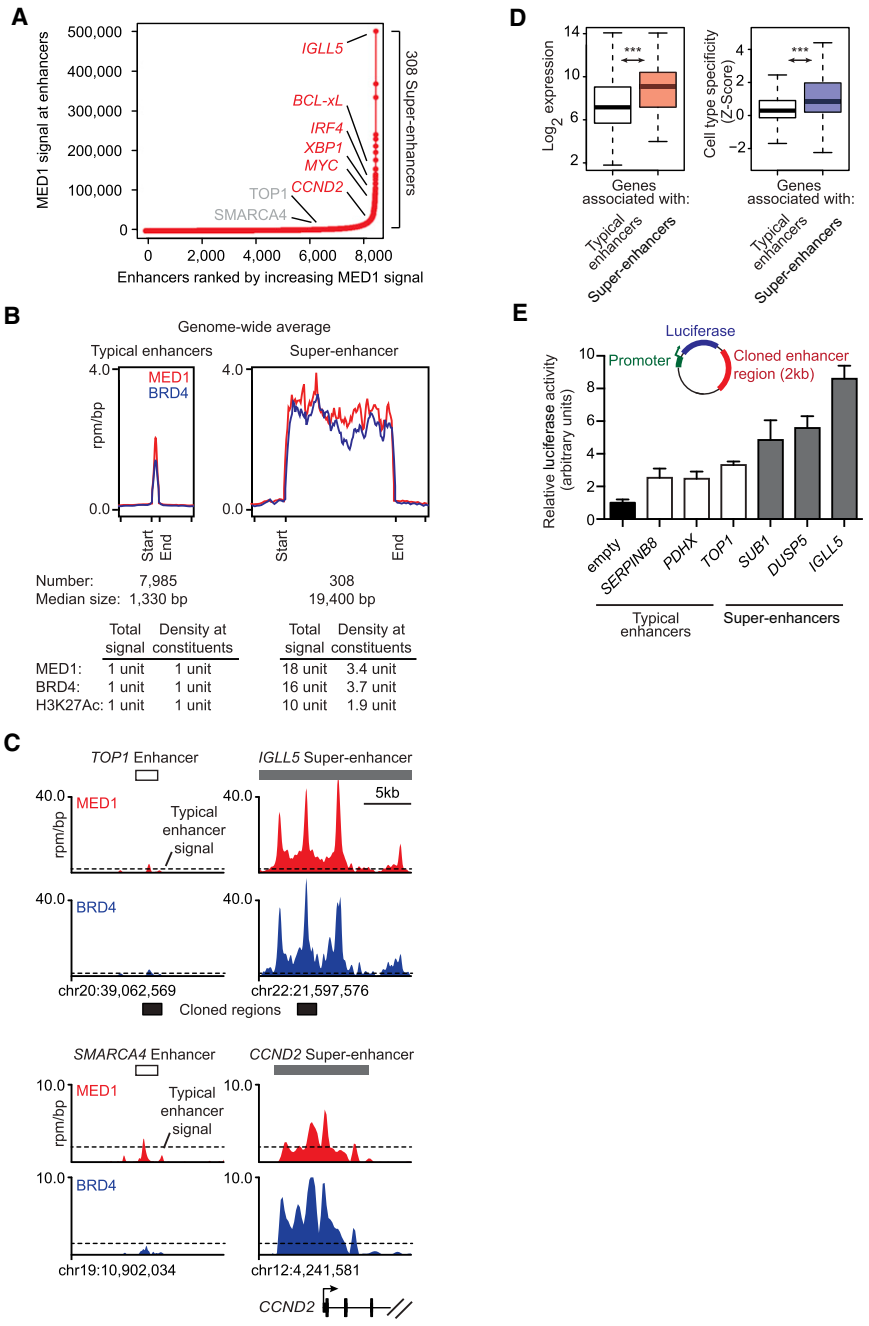

Figure 2. Super-Enhancers Identified in Multiple Myeloma

(A) Total MED1 ChIP-seq signal in units of reads per million in enhancer regions for all enhancers in MM1.S. Enhancers are ranked by increasing MED1 ChIP-seq signal.

(B) Metagene representation of global MED1 (red line) and BRD4 (blue line) occupancy at typical enhancers and super-enhancers. The x axis shows the start and end of the enhancer (left) or super-enhancer (right) regions flanked by ±5 kb of adjacent sequence. Enhancer and super-enhancer regions on the x axis are relatively scaled. The y axis shows the average signal in units of rpm/bp.

(C) Gene tracks of MED1 (top) and BRD4 (bottom) ChIP-seq occupancy at the typical enhancer upstream of *TOP1*, the super-enhancer downstream of *IGLL5*, the typical enhancer upstream of *SMARCA4*, and the super-enhancer overlapping the *CCND2* gene TSS. The x axis shows genomic position, and super-enhancer-containing regions are depicted with a gray box. The y axis shows signal of ChIP-seq occupancy in units of rpm/bp.

(D) Left: box plots of expression values for genes with proximal typical enhancers (white) or with proximal super-enhancers (pink). The y axis shows expression value in Log2 arbitrary units. Right: box plots of cell-type specificity values for genes with proximal typical enhancers (white) or with proximal super-enhancers (purple). The y axis shows the *Z* score of the Jensen-Shannon (JS) divergence statistic for genes, with higher values corresponding to a more cell-type-specific pattern of expression. Changes between expression levels are significant (two-tailed Welch's t test, $p < 2 \times 10^{-16}$), as are changes between cell-type-specificity levels (two-tailed Welch's t test, $p = 1 \times 10-14$).

(E) Bar graph depicting luciferase activity of reporter constructs containing cloned fragments of typical enhancers and super-enhancers in MM1.S cells. 2 kb fragments of three super-enhancers, IGLL5, DUSP5, and SUB1, and three typical enhancers, PDHX, SERPINB8, and TOP1, ranked 1, 129, 227, 2352, 4203, and 4794, respectively, in terms of MED1 occupancy, were cloned into reporter plasmids downstream of the luciferase gene, driven by a minimal *MYC* promoter. Luciferase activity is represented as fold over empty vector. Error bars represent SD of triplicate experiments.

See also Figure S2 and Data S1.

chemoresistance (Beroukhim et al., 2010). We conclude that super-enhancers are frequently associated with genes that feature prominently in the biology of MM and other human cancers.

Inhibition of BRD4 Leads to Displacement of BRD4 Genome Wide

BRD4 interacts with chromatin-associated proteins such as transcription factors, the Mediator complex, and acetylated histones (Dawson et al., 2011; Dey et al., 2003; Jang et al., 2005; Jiang et al., 1998; Wu and Chiang, 2007; Wu et al., 2013). Previous studies have shown that treatment of MM1.S cells with JQ1 leads to reduced levels of BRD4 at the *IgH* enhancer that drives *MYC* expression (Delmore et al., 2011), but it is not clear whether such treatment causes a general reduction in the levels of BRD4 associated with the genome. We found that treatment of MM1.S cells with 500 nM JQ1 for 6 hr reduced the levels of BRD4 genome wide by ~70% (Figures 4A and 4B). This reduction in BRD4 occupancy was evident both by inspection of individual gene tracks (Figure 4C) and through global analysis of the average effects at enhancers and TSSs

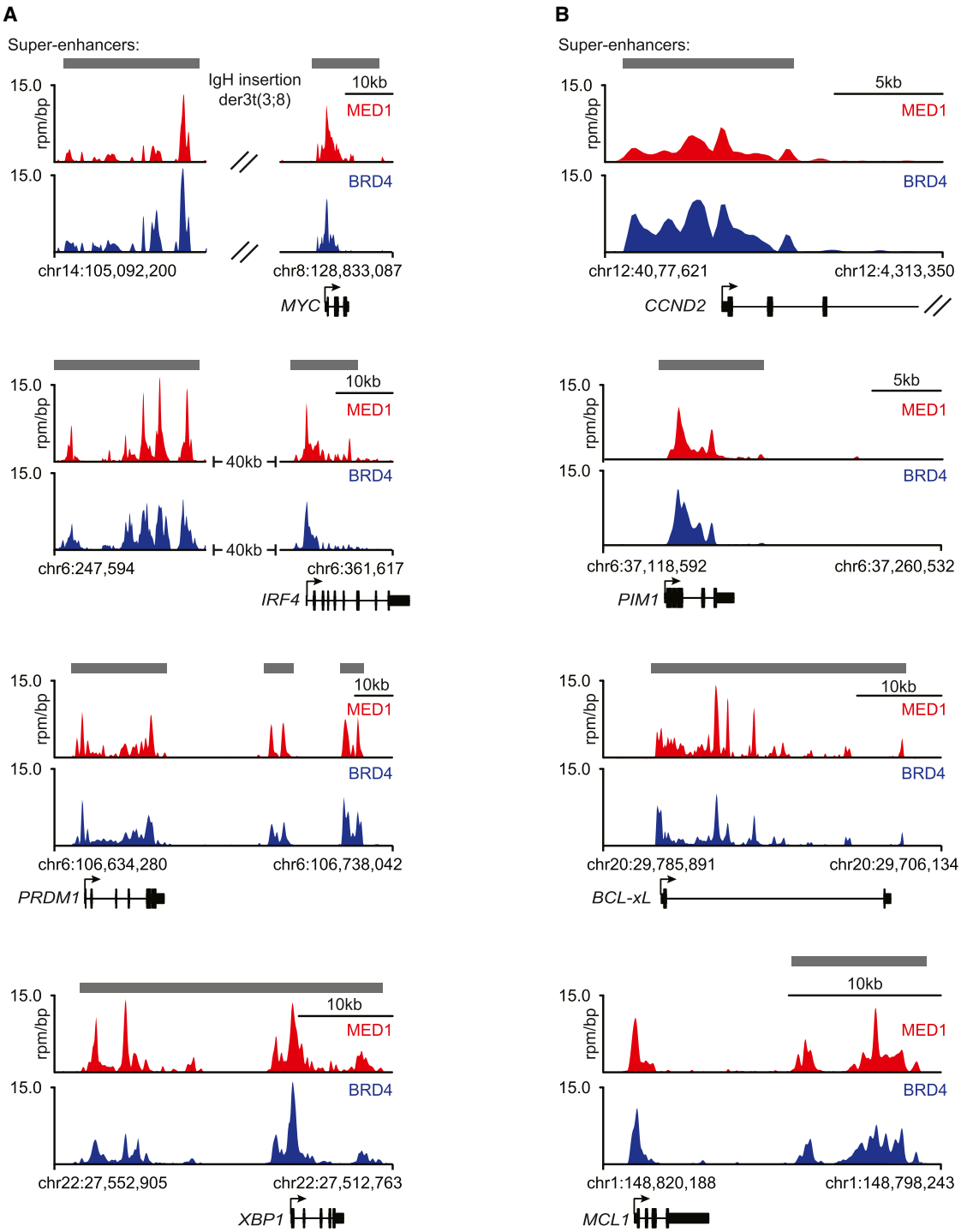

Figure 3. Super-Enhancers Are Associated with Key Multiple Myeloma Genes

(A and B) Gene tracks of MED1 and BRD4 ChIP-seq occupancy at super-enhancers near genes with important roles in MM biology (A) or genes with important roles in cancer (B). Super-enhancers are depicted in gray boxes over the gene tracks. The x axis shows genomic position, and super-enhancer-containing regions are depicted with a gray box. The y axis shows signal of ChIP-seq occupancy in units of rpm/bp.

(Figure 4D). JQ1 treatment led to ~60% reduction in BRD4 signal at enhancers and ~90% reduction at promoters (Figure 4D). The reduction in BRD4 was more profound at super-enhancers such as those associated with *IgH-MYC* and *CCND2* (Figure 4E), where the loss of BRD4 was nearly complete. We conclude that BET bromodomain inhibition of BRD4

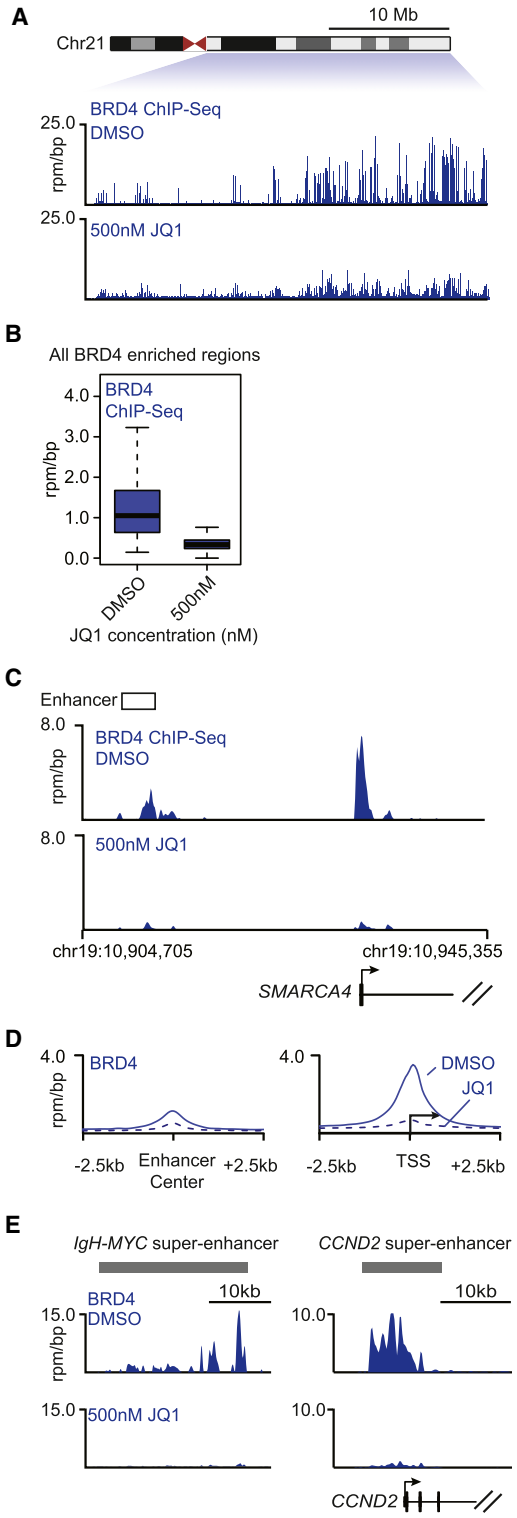

Figure 4. Inhibition of BRD4 Leads to Loss of BRD4 Genome Wide

(A) Tracks showing BRD4 ChIP-seq occupancy on the 35 Mb right arm of chromosome 21 after DMSO (top) or 500 nM JQ1 (bottom) treatment. The chromosome 21 ideogram is displayed above the gene tracks with the relevant region highlighted in blue. The x axis of the gene tracks shows genomic position, and the y axis shows BRD4 ChIP-seq signal in units of rpm/bp.

(B) Box plot showing the distributions of BRD4 ChIP-seq signal at BRD4-enriched regions after DMSO (left) or 500 nM JQ1 (right) treatment. BRD4-enriched regions were defined in MM1.S cells treated with DMSO. The y axis shows BRD4 ChIP-seq signal in units of rpm/bp. The loss of BRD4 occupancy at BRD4-enriched regions after JQ1 is highly significant (p value $< 1 \times 10^{-16}$, Welch's t test).

(C) Gene tracks of BRD4 ChIP-seq occupancy at the enhancer (left) and promoter (right) of *SMARCA4* in MM1.S cells after DMSO (top) or 500 nM JQ1 (bottom) treatment for 6 hr. The x axis shows genomic position, and enhancer-containing regions are depicted with a white box. The y axis shows signal of ChIP-seq occupancy in units of rpm/bp.

(D) Metagene representation of global BRD4 occupancy at enhancers and promoters after DMSO (solid line) or 500 nM JQ1 (dotted line) treatment. The x axis shows the ±2.5 kb region flanking either the center of enhancer regions (left) or the TSS of active genes. The y axis shows the average background subtracted ChIP-seq signal in units of rpm/bp.

(E) Gene tracks of BRD4 binding at super-enhancers after DMSO (top) or 500 nM JQ1 (bottom) treatment. The x axis shows genomic position, and super-enhancer-containing regions are depicted with a gray box. The y axis shows signal of ChIP-seq occupancy in units of rpm/bp.

leads to reduced levels of BRD4 at enhancers and promoters throughout the genome in MM1.S cells.

Transcription of Super-Enhancer-Associated Genes Is Highly Sensitive to BRD4 Inhibition

Enhancers are formed through cooperative and synergistic binding of multiple transcription factors and coactivators (Carey, 1998; Carey et al., 1990; Giese et al., 1995; Kim and Maniatis, 1997; Thanos and Maniatis, 1995). As a consequence of this binding behavior, enhancers bound by many cooperatively interacting factors lose activity more rapidly than enhancers bound by fewer factors when the levels of enhancer-bound factors are reduced (Giniger and Ptashne, 1988; Griggs and Johnston, 1991). The presence of super-enhancers at *MYC* and other key genes associated with MM led us to consider the hypothesis that super-enhancers are more sensitive to reduced levels of BRD4 than typical enhancers and that genes associated with super-enhancers might then experience a greater reduction of transcription than genes with average enhancers when BRD4 is inhibited (Figure 5A).

To test this hypothesis, we first examined the effects of various concentrations of JQ1 on BRD4 occupancy genome wide (Figure 5B). JQ1 had little effect on MM1.S cell viability when treated for 6 hr at these various concentrations, whereas at later time points, JQ1 had a significant antiproliferative effect (Figure 5C). As expected, MYC protein levels were significantly depleted by exposure of MM1.S cells to 50 nM or greater doses of JQ1 for 6 hr (Figure 6D) (Delmore et al., 2011). In contrast, JQ1 did not affect total BRD4 protein levels within the cells and did not significantly reduce ChIP efficiency (Figure 5E). When BRD4 occupancy was examined genome wide in cells exposed to increasing concentrations of JQ1, it was evident that super-enhancers showed a greater loss of BRD4 occupancy than typical enhancer regions (Figure 5F). For example, the *IgH* super-enhancer showed significantly greater reduction in BRD4 occupancy in cells treated with 5 nM or 50 nM JQ1 than typical enhancer regions such as that upstream of *SMARCA4* (Figure 5G). Ultimately, virtually all BRD4 occupancy was lost at the *IgH* super-enhancer (97% reduction versus DMSO control)

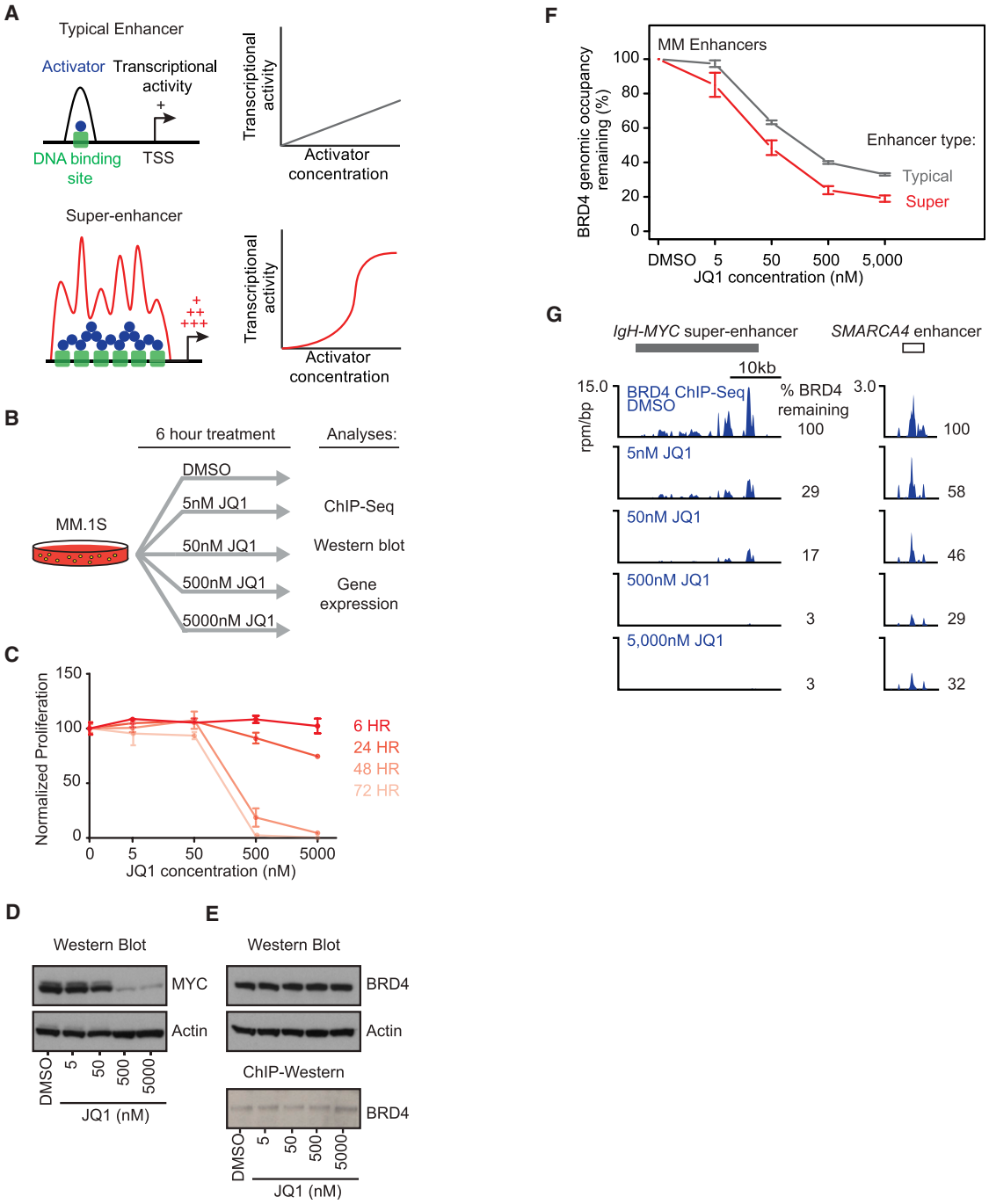

Figure 5. BRD4 Occupancy at Super-Enhancers Is Highly Sensitive to Bromodomain Inhibition

(A) Schematic example of how cooperative interactions of enhancer-associated factors at super-enhancers lead to both higher transcriptional output and increased sensitivity to factor concentration.

(B) Measuring the effects of various concentrations of JQ1 genome wide on BRD4 occupancy. Schematic depicting the experimental procedure.

(C) Short-term JQ1 treatment (6 hr) has little effect on MM1.S cell viability. JQ1 sensitivity of MM1.S cells by measurement of ATP levels (CellTiterGlo) after 6, 24, 48, and 72 hr of treatment with JQ1 (5, 50, 500, or 5,000 nM) or vehicle (DMSO, 0.05%). Error bars represent the SD of triplicate experiments.

(D) Western blot of relative MYC levels after 6 hr of JQ1 or DMSO treatment.

(E) Western blot of relative BRD4 levels after 6 hr of JQ1 or DMSO treatment. ChIP-western blot of the relative levels of immunoprecipitated BRD4 after 6 hr of JQ1 or DMSO treatment.

(F) Line graph showing the percentage of BRD4 occupancy remaining after 6 hr treatment at various JQ1 concentrations for typical enhancers (gray line) or super-enhancers (red line). The y axis shows the fraction of BRD4 occupancy remaining versus DMSO. The x axis shows different JQ1 concentrations (DMSO [none], 5 nM, 50 nM, and 500 nM). Error bars represent 95% confidence intervals of the mean (95% CI).

(legend continued on next page)

after treatment with 500 nM JQ1, whereas loss of BRD4 occupancy at the typical enhancer for *SMARCA4* was less pronounced (71% reduction versus DMSO control) (Figure 5G).

We next investigated whether genes associated with super-enhancers might experience a greater reduction of transcription than genes with average enhancers when BRD4 is inhibited. As expected, treatment of MM1.S cells with 500 nM JQ1 led to progressive reduction in global messenger RNA (mRNA) levels over time (Figures 6A and S3A). Similarly, treatment with increasing concentrations of JQ1 caused progressive reductions in global mRNA levels (Figures 6A and S3B). There was a selective depletion of mRNAs from super-enhancer-associated genes that occurred in both temporal (Figure 6B) and concentration-dependent manners (Figure 6C). Notably, *MYC* and *IRF4* mRNA levels were more rapidly depleted than other mRNAs that are expressed at similar levels (Figure 6D). The levels of transcripts from super-enhancer-associated genes were somewhat more affected than those from genes that have multiple typical enhancers bound by BRD4 (Figures S3C and S3D). Thus, BET bromodomain inhibition preferentially impacts transcription of super-enhancer-driven genes.

To further test the model that super-enhancers are responsible for the special sensitivity to BRD4 inhibition, we transfected MM1.S cells with luciferase reporter constructs containing super-enhancer and typical enhancer fragments and examined the effects of various JQ1 concentrations on luciferase activity. Upon treatment with JQ1, MM1.S cells transfected with a super-enhancer reporter experienced a greater reduction in luciferase activity than those transfected with a typical enhancer reporter (Figure 6E). Interestingly, the dose-response curve observed for luciferase activity of the super-enhancer construct is consistent with that expected for enhancers that are bound cooperatively by multiple factors (Figure 5A) (Giniger and Ptashne, 1988; Griggs and Johnston, 1991). These results are also consistent with the model that super-enhancers are responsible for the special sensitivity of gene transcription to BRD4 inhibition.

BRD4 Inhibition and Transcription Elongation

At active genes, enhancers and core promoters are brought into close proximity, so factors associated with enhancers can act on the transcription apparatus in the vicinity of TSSs and thereby influence initiation or elongation. BRD4 is known to interact with Mediator and P-TEFb and to be involved in the control of transcriptional elongation by RNA Pol II (Conaway and Conaway, 2011; Dawson et al., 2011; Jang et al., 2005; Krueger et al., 2010; Rahman et al., 2011; Yang et al., 2005). This suggests that the preferential loss of BRD4 from super-enhancers might affect the levels of Mediator and P-TEFb at these sites and, furthermore, that the reduced levels of mRNAs from super-enhancer-associated genes might be due to an effect on transcription elongation.

To test these predictions, we carried out ChIP-seq for the Mediator component MED1 and the catalytic subunit of the P-TEFb complex CDK9 in MM1.S cells treated with DMSO or 500 nM JQ1 for 6 hr. In control cells, MED1 and CDK9 were found at enhancers and promoters of active genes throughout the MM genome, as expected (Figures 1A, 1B, and S3E). In cells treated with JQ1, reduced levels of MED1 and CDK9 were observed primarily at enhancers, with the greatest loss at super-enhancers (Figure 6F). As many super-enhancers span contiguous regions that encompass or overlap the TSS, we analyzed MED1 and CDK9 loss in either TSS proximal or TSS distal regions of super-enhancers and again observed loss of MED1 and CDK9 predominantly at TSS distal regions (Figure S3F). We conclude that inhibition of BRD4 genomic binding leads to a marked reduction in the levels of Mediator and P-TEFb at genomic regions distal to TSSs, with the greatest reduction occurring at super-enhancers.

To determine whether reduced levels of BRD4 lead to changes in transcription elongation, we quantified changes in transcription elongation by performing ChIP-seq of RNA Pol II before and after treatment of MM1.S cells with 500 nM JQ1. We then calculated the fold loss of RNA Pol II occupancy in the gene body regions for all transcriptionally active genes and found that more than half of these genes show a decrease in elongating RNA Pol II density after JQ1 treatment (Figure 6G). Importantly, genes associated with super-enhancers showed a greater decrease of RNA Pol II in their elongating gene body regions compared to genes associated with typical enhancers (Figures 6H and S3G). Inspection of individual gene tracks revealed pronounced elongation defects at super-enhancer-associated genes such as *MYC* and *IRF4*, with the greatest effects observed with *MYC* (Figures 6I and 6J). Thus, the selective effects of JQ1 on the transcription of *MYC* and other super-enhancer-associated genes can be explained, at least in part, by the sensitivity of super-enhancers to reduced levels of BRD4, which leads to a pronounced effect on pause release and transcription elongation.

Super-Enhancers Are Associated with Disease-Critical Genes in Other Cancers

To map enhancers and to determine whether super-enhancers occur in additional tumor types, we investigated the genome-wide occupancy of Mediator (MED1), BRD4, and the enhancer-associated histone modification H3K27Ac using ChIP-seq in glioblastoma multiforme (GBM) and small-cell lung cancer (SCLC) (Figure 7). Mediator (MED1) occupancy was used to identify enhancer elements because enhancer-bound transcription factors bind directly to Mediator (Borggrefe and Yue, 2011; Conaway and Conaway, 2011; Kornberg, 2005; Malik and Roeder, 2010; Taatjes, 2010) and because it has proven to produce high-quality evidence for enhancers in mammalian cells (Kagey et al., 2010). Global occupancy of BRD4 and H3K27Ac was used as corroborative evidence to identify enhancer elements (Figure S4 and Table S4). Analysis of the regions occupied by Mediator revealed that, as in

(G) Gene tracks of BRD4 ChIP-seq occupancy after various concentrations of JQ1 treatment at the *IgH-MYC*-associated super-enhancer (left) and the *SMARCA4*-associated typical enhancer (right). The x axis shows genomic position, and gray boxes depict super-enhancer regions. The y axis shows signal of ChIP-seq occupancy in units of rpm/bp. The percent of BRD4 remaining after each concentration of JQ1 treatment is annotated to the right of the gene tracks.

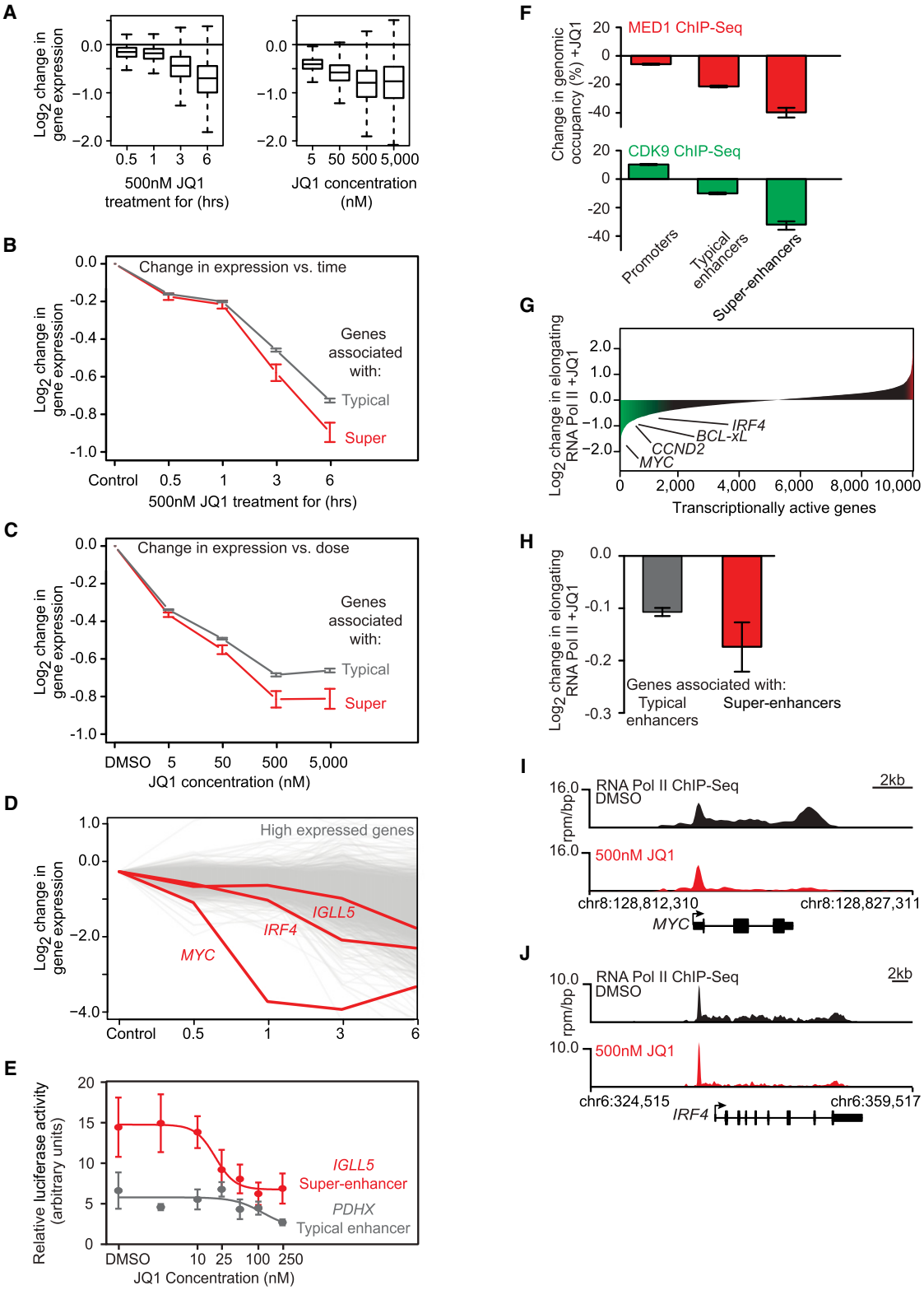

Figure 6. JQ1 Causes Disproportionate Loss of Transcription at Super-Enhancer Genes

(A) Box plots showing the Log_2 change in gene expression for all actively transcribed genes in JQ1-treated versus control cells for a time course of cells treated with 500 nM JQ1 (left) or for a concentration course of cells treated for 6 hr with varying amounts of JQ1 (right). The y axis shows the Log_2 change in gene expression versus untreated control cells (left graph) or control cells treated with DMSO for 6 hr (right graph).

(legend continued on next page)

MM1.S cells, large genomic domains were occupied by this co-activator in both GBM and SCLC (Figures 7A, 7B, 7D, and 7E). The median super-enhancer was 30 kb in GBM cells and 11 kb in SCLC cells (Figures 7B and 7E). As in MM1.S cells, these GBM and SCLC super-enhancers were an order or magnitude larger and showed a commensurate increase in MED1, BRD4, and H3K27Ac levels when compared to normal enhancers (Figures 7B and 7E).

The super-enhancers in GBM and SCLC were found to be associated with many well-known tumor-associated genes (Figures 7C and 7F and Table S5). In GBM, super-enhancers were associated with genes encoding three transcription factors (*RUNX1*, *FOSL2*, and *BHLHE40*) critical for mesenchymal transformation of brain tumors (Carro et al., 2010); the super-enhancers associated with *BHLHE40* are shown in Figure 7C. *BCL3*, which associates with NF-κB and is deregulated in many blood and solid tumor types, is associated with a super-enhancer in GBM (Figure 7C) (Maldonado and Melendez-Zajgla, 2011). In SCLC, a super-enhancer is associated with the *INSM1* gene, which encodes a transcription factor involved in neuronal development that is highly expressed in neuroendocrine tissue and tumors such as SCLC (Figure 7F) (Pedersen et al., 2003). A super-enhancer is also associated with the *ID2* gene, which is highly expressed in SCLCs and encodes a protein that interacts with the well-known retinoblastoma tumor suppressor (Figure 7F) (Pedersen et al., 2003; Perk et al., 2005). These results indicate that super-enhancers are likely to associate with critical tumor oncogenes in diverse tumor types.

DISCUSSION

Chromatin regulators have become attractive targets for cancer therapy, but many of these regulators are expressed in a broad range of healthy cells and contribute generally to gene expression. Thus, it is unclear how inhibition of a global chromatin regulator such as BRD4 might produce selective effects, such as at the *MYC* oncogene (Delmore et al., 2011). We have found that key regulators of tumor cell state in MM1.S cells are associated with large enhancer domains, characterized by disproportionately high levels of BRD4 and Mediator. These super-enhancers are more sensitive to perturbation than typical enhancers, and the expression of the genes associated with super-enhancers is preferentially affected. Thus, the preferential loss of BRD4 at super-enhancers associated with the *MYC* oncogene and other key tumor-associated genes can explain the gene-selective effects of JQ1 treatment in these cells.

BRD4 is an excellent example of a chromatin regulator that is expressed in a broad range of healthy cells and contributes generally to gene expression. Most cell types for which RNA-seq data are available express the *BRD4* gene. ChIP-seq data revealed that BRD4 generally occupies the enhancer and promoter elements of active genes with the Mediator coactivator in MM1.S cells (Figure 1). These results eliminate the model that BRD4 is exclusively associated with a small set of genes that are thereby rendered inactive by the BRD4 inhibitor JQ1 and instead suggest that the gene-specific effects of the small molecule have other causes.

We have found that ~3% of the enhancers in MM1.S cells are exceptionally large and are occupied by remarkably high amounts of BRD4 and Mediator. These super-enhancers are generally an order of magnitude larger and contain an order of magnitude more BRD4, Mediator, and histone marks associated with enhancers (H3K27Ac) than typical enhancers. Our results suggest that super-enhancers are collections of closely spaced enhancers that can collectively facilitate high levels of transcription from adjacent genes. Importantly, the super-enhancers are associated with the *MYC* oncogene and additional genes such as *IGLL5*, *IRF4*, *PRDM1/BLIMP-1*, and *XBP1* that feature prominently in MM biology.

Cooperative and synergistic binding of multiple transcription factors and coactivators occurs at enhancers. Enhancers bound by many cooperatively interacting factors can lose activity more rapidly than enhancers bound by fewer factors when the levels of enhancer-bound factors are reduced (Giniger and Ptashne, 1988; Griggs and Johnston, 1991). The presence of super-enhancers at *MYC* and other key genes associated with MM led us to test the hypothesis that super-enhancers are more sensitive to reduced levels of BRD4 than average enhancers. We

(B and C) Line graph showing the Log2 change in gene expression versus control cells after JQ1 treatment in a time- (B) or dose (C)-dependent manner for genes associated with typical enhancers (gray line) or genes associated with super-enhancers (red line). The y axis shows the Log2 change in gene expression of JQ1 treated versus untreated control cells. The x axis shows time of 500 nM JQ1 treatment (B) or JQ1 treatment concentration at 6 hr (C). Error bars represent 95% confidence intervals of the mean (95% CI).

(D) Graph showing the Log_2 change in gene expression after JQ1 treatment over time for genes ranked in the top 10% of expression in MM1.S cells. Each line represents a single gene, with the *MYC* and *IRF4* genes drawn in red. The y axis shows the Log_2 change in gene expression of JQ1-treated versus untreated control cells. The x axis shows time of 500 nM JQ1 treatment.

(E) Line graph showing luciferase activity after JQ1 treatment at various concentrations for luciferase reporter constructs containing either a fragment from the *IGLL5* super-enhancer (red line) or the *PDHX* typical enhancer (gray line). The y axis represents relative luciferase activity in arbitrary units. The x axis shows JQ1 concentrations. Error bars are SEM.

(F) Bar graphs showing the percentage loss of either MED1 (top, red) or CDK9 (bottom, green) at promoters, typical enhancers, and super-enhancers. Error bars represent 95% CI.

(G) Graph of loss of RNA Pol II density in the elongating gene body region for all transcriptionally active genes in MM1.S cells after 6 hr of 500 nM JQ1 treatment. Genes are ordered by decrease in elongating RNA Pol II in units of Log_2 fold loss. Genes with a greater than 0.5 Log_2 fold change in elongating RNA Pol II are shaded in green (loss) or red (gain). The amount of RNA Pol II loss is indicated for select genes.

(H) Bar graph showing the Log_2 fold change in RNA Pol II density in elongating gene body regions after 6 hr of 500 nM JQ1 treatment for genes with typical enhancers (left, gray) or genes with super-enhancers (red, right). Error bars represent 95% confidence intervals of the mean (95% CI).

(I and J) Gene tracks of RNA Pol II ChIP-seq occupancy after DMSO (black) or 500 nM JQ1 treatment (red) at the super-enhancer proximal *MYC* gene (I) and *IRF4* gene (J). The y axis shows signal of ChIP-seq occupancy in units of rpm/bp.

See also Figure S3.

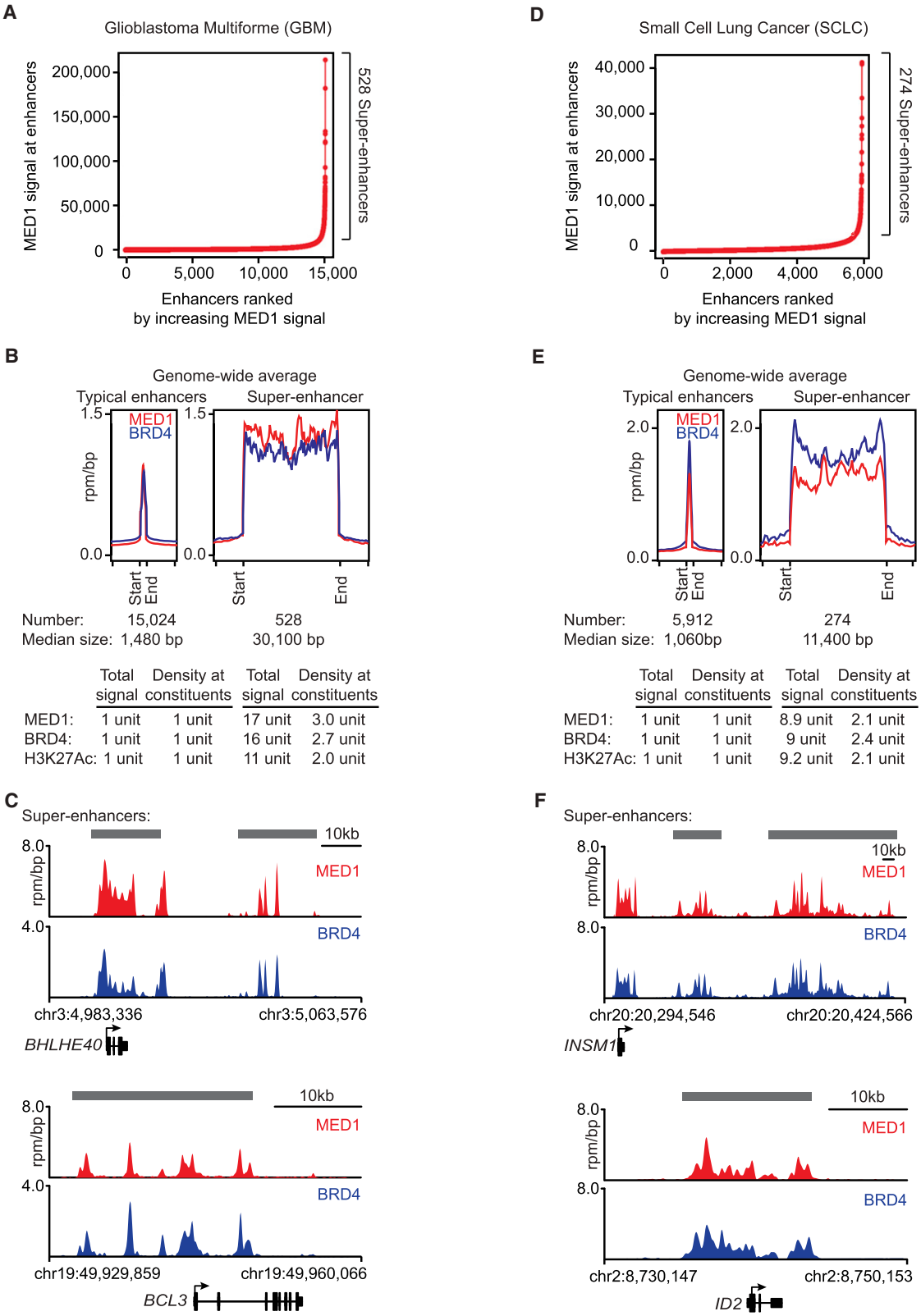

(legend on next page)

found that treatment of these tumor cells with the BET-bromodomain inhibitor JQ1 leads to preferential loss of BRD4 at super-enhancers. In addition, this decrease in BRD4 occupancy is accompanied by a corresponding loss of MED1 and CDK9 at super-enhancers. Consequent transcription elongation defects and mRNA decreases preferentially impact super-enhancer-associated genes, with an especially profound effect at the *MYC* oncogene.

Super-enhancers are not restricted to MM cells. We have identified super-enhancers in two additional tumor types, small-cell lung cancer and glioblastoma multiforme. Super-enhancers identified in these cell types have characteristics similar to those found in MM1.S; they span large genomic regions and contain exceptional amounts of Mediator and BRD4. These super-enhancers are also associated with important tumor genes in both cell types. In GBM cells, *BHLHE40* and *BCL3* are known to be important in tumor biology and are each associated with super-enhancers in this cell type. In H2171 SCLC cells, super-enhancers are associated with *INSM1* and *ID2*, which are frequently overexpressed in SCLC. In fact, super-enhancers are not restricted to tumor cells and have been identified in several additional cell types in which they similarly associate with key cell identity genes (Whyte et al., 2013 [this issue of *Cell*]).

Our results demonstrate that super-enhancers occupied by BRD4 regulate critical oncogenic drivers in MM and show that BRD4 inhibition leads to preferential disruption of these super-enhancers. This insight into the mechanism by which BRD4 inhibition causes selective loss of oncogene expression in this highly malignant blood cancer may have implications for future drug development in oncology. Tumor cells frequently become addicted to oncogenes, thus becoming unusually reliant on high-level expression of these genes (Cheung et al., 2011; Chin et al., 1999; Felsher and Bishop, 1999; Garraway and Sellers, 2006; Garraway et al., 2005; Jain et al., 2002; Weinstein, 2002). Thus, preferential disruption of super-enhancer function may be a general approach to selectively inhibiting the oncogenic drivers of many tumor cells.

EXPERIMENTAL PROCEDURES

Cell Culture

MM1.S MM cells (CRL-2974 ATCC) and U-87 MG glioblastoma cells (HTB-14 ATCC) were purchased from ATCC. H2171 small-cell lung carcinoma cells (CRL-5929 ATCC) were kindly provided by John Minna, UT Southwestern. MM1.S and H2171 cells were propagated in RPMI-1640 supplemented with 10% fetal bovine serum and 1% GlutaMAX (Invitrogen, 35050-061). U-87 MG cells were cultured in Eagle's minimum essential medium (EMEM) modified to contain Earle's Balanced Salt Solution, nonessential amino acids, 2 mM L-glutamine, 1 mM sodium pyruvate, and 1,500 mg/l sodium bicarbonate. Cells were grown at 37°C and 5% CO_2.

For JQ1 treatment experiments, cells were resuspended in fresh media containing JQ1 (5 nM, 50 nM, 500 nM, and 5,000 nM) or vehicle (DMSO, 0.05%) and treated for a duration of 6 hr, unless otherwise indicated.

ChIP-Seq

ChIP was carried out as described in Lin et al. (2012). Additional details are provided in Extended Experimental Procedures. Antibodies used are as follows: total RNA Pol II (Rpb1 N terminus), Santa Cruz sc-899 lot K0111; MED1, Bethyl Labs A300-793A lot A300-793A-2; BRD4, Bethyl Labs A301-985A lot A301-985A-1; CDK9, Santa Cruz Biotechnology sc-484, lot D1612. ChIP-seq data sets of H3K4Me3 and H3K27Ac in MM1.S and MED1 and H3K27Ac in U-87 MG and H2171 were previously published (Lin et al., 2012).

Luciferase Reporter Assays

A minimal Myc promoter was amplified from human genomic DNA and cloned into the SacI and HindIII sites of the pGL3 basic vector (Promega). Enhancer fragments were likewise amplified from human genomic DNA and cloned into the BamHI and SalI sites of the pGL3-pMyc vector. All cloning primers are listed in Table S6. Constructs were transfected into MM1.S cells using Lipofectamine 2000 (Invitrogen). The pRL-SV40 plasmid (Promega) was co-transfected as a normalization control. Cells were incubated for 24 hr, and luciferase activity was measured using the Dual-Luciferase Reporter Assay System (Promega). For the JQ1 concentration course, cells were resuspended in fresh media containing various concentrations of JQ1 24 hr after transfection and were incubated for an additional 6 hr before harvesting. Luminescence measurements were made using the Dual-Luciferase Reporter Assay System (Promega) on a Wallac EnVision (Perkin Elmer) plate reader.

Cell Viability Assays

Cell viability was measured using the CellTiterGlo assay kit (Promega, G7571). MM1.S cells were resuspended in fresh media containing JQ1 (5 nM, 50 nM, 500 nM, and 1,000 nM) or vehicle (DMSO, 0.05%) and then plated in 96-well plates at 10,000 cells/well in a volume of 100 μl. Viability was measured after 6, 24, 48, and 72 hr incubations by addition of CellTiter Glo reagent and luminescence measurement on a Tecan Safire^2 plate reader.

Western Blotting

Western blots were carried out using standard protocols. Antibodies used are as follows: c-Myc (Epitomics, category: 1472-1), BRD4 (Epitomics, category: 5716-1) or β-actin (Sigma, clone AC-15, A5441).

Data Analysis

All ChIP-seq data sets were aligned using Bowtie (version 0.12.9) (Langmead et al., 2009) to build version NCBI36/HG18 of the human genome. Individual data set GEO accession IDs and background data sets used can be found in Table S7.

ChIP-seq read densities in genomic regions were calculated as in Lin et al. (2012). We used the MACS version 1.4.2 (model-based analysis of ChIP-seq) (Zhang et al., 2008) peak finding algorithm to identify regions of ChIP-seq enrichment over background. A p value threshold of enrichment of 1×10^{-9} was used for all data sets.

Active enhancers were defined as regions of ChIP-seq enrichment for the mediator complex component MED1 outside of promoters (e.g., a region not contained within ±2.5 kb region flanking the promoter). In order to accurately capture dense clusters of enhancers, we allowed MED1 regions within 12.5 kb of one another to be stitched together. To identify super-enhancers, we first

Figure 7. Super-Enhancers Are Associated with Key Genes in Other Cancers

(A and D) Total MED1 ChIP-seq signal in units of reads per million in enhancer regions for all enhancers in (A) the GBM cell line U-87 MG or (D) the SCLC cell line H2171. Enhancers are ranked by increasing MED1 ChIP-seq signal.

(B and E) Metagene representation of global MED1 and BRD4 occupancy at (B) typical GMB enhancers and super-enhancers or (E) typical SCLC enhancers and super-enhancers. The x axis shows the start and end of the enhancer (left) or super-enhancer (right) regions flanked by ±5 kb of adjacent sequence. Enhancer and super-enhancer regions on the x axis are relatively scaled. The y axis shows the average signal in units of rpm/bp.

(C and F) Gene tracks of MED1 and BRD4 ChIP-seq occupancy at (C) super-enhancers near *BHLHE40* and *BCL3*, genes with important roles in GBM, or at (F) super-enhancers near *INSM1* and *ID2*, genes with important roles in SCLC. Super-enhancers are depicted in gray boxes over the gene tracks.

See also Figure S4.

ranked all enhancers by increasing total background subtracted ChIP-seq-occupancy of MED1 (x axis) and plotted the total background subtracted ChIP-seq occupancy of MED1 in units of total rpm (y axis). This representation revealed a clear inflection point in the distribution of MED1 at enhancers. We geometrically defined the inflection point and used it to establish the cutoff for super-enhancers (see Extended Experimental Procedures).

ACCESSION NUMBERS

The GEO accession number for the ChIP-seq and gene expression data reported in this paper is GSE44931 (http://www.ncbi.nlm.nih.gov/geo/).

SUPPLEMENTAL INFORMATION

Supplemental Information includes Extended Experimental Procedures, four figures, one data file, and seven tables and can be found with this article online at http://dx.doi.org/10.1016/j.cell.2013.03.036.

ACKNOWLEDGMENTS

We thank Zi Peng Fan for bioinformatics support; Michael R. McKeown for help with cell viability assays; Jun Qi for providing JQ1; Tom Volkert, Jennifer Love, Sumeet Gupta, and Jeong-Ah Kwon at the Whitehead Genome Technologies Core for Solexa sequencing; and members of the Young, Bradner, and Vakoc labs for helpful discussion. This work was supported by a Swedish Research Council Postdoctoral Fellowship VR-B0086301 (J.L.), the Damon-Runyon Cancer Research Foundation (J.E.B.), a Burroughs-Welcome CAMS award and NCI Cancer Center Support Grant Development Fund CA45508 (C.R.V.), and National Institutes of Health grants HG002668 (R.A.Y.) and CA146445 (R.A.Y., T.I.L.). R.A.Y. and J.E.B. are founders, J.L. and D.A.O. have become employees, and C.R.V. is a scientific advisor of Syros Pharmaceuticals.

Received: November 16, 2012
Revised: February 25, 2013
Accepted: March 25, 2013
Published: April 11, 2013

REFERENCES

Baylin, S.B., and Jones, P.A. (2011). A decade of exploring the cancer epigenome - biological and translational implications. Nat. Rev. Cancer *11*, 726–734.

Bergsagel, P.L., Kuehl, W.M., Zhan, F., Sawyer, J., Barlogie, B., and Shaughnessy, J., Jr. (2005). Cyclin D dysregulation: an early and unifying pathogenic event in multiple myeloma. Blood *106*, 296–303.

Beroukhim, R., Mermel, C.H., Porter, D., Wei, G., Raychaudhuri, S., Donovan, J., Barretina, J., Boehm, J.S., Dobson, J., Urashima, M., et al. (2010). The landscape of somatic copy-number alteration across human cancers. Nature *463*, 899–905.

Borggrefe, T., and Yue, X. (2011). Interactions between subunits of the Mediator complex with gene-specific transcription factors. Semin. Cell Dev. Biol. *22*, 759–768.

Carey, M. (1998). The enhanceosome and transcriptional synergy. Cell *92*, 5–8.

Carey, M., Leatherwood, J., and Ptashne, M. (1990). A potent GAL4 derivative activates transcription at a distance in vitro. Science *247*, 710–712.

Carrasco, D.R., Sukhdeo, K., Protopopova, M., Sinha, R., Enos, M., Carrasco, D.E., Zheng, M., Mani, M., Henderson, J., Pinkus, G.S., et al. (2007). The differentiation and stress response factor XBP-1 drives multiple myeloma pathogenesis. Cancer Cell *11*, 349–360.

Carro, M.S., Lim, W.K., Alvarez, M.J., Bollo, R.J., Zhao, X., Snyder, E.Y., Sulman, E.P., Anne, S.L., Doetsch, F., Colman, H., et al. (2010). The transcriptional network for mesenchymal transformation of brain tumours. Nature *463*, 318–325.

Chepelev, I., Wei, G., Wangsa, D., Tang, Q., and Zhao, K. (2012). Characterization of genome-wide enhancer-promoter interactions reveals co-expression of interacting genes and modes of higher order chromatin organization. Cell Res. *22*, 490–503.

Cheung, H.W., Cowley, G.S., Weir, B.A., Boehm, J.S., Rusin, S., Scott, J.A., East, A., Ali, L.D., Lizotte, P.H., Wong, T.C., et al. (2011). Systematic investigation of genetic vulnerabilities across cancer cell lines reveals lineage-specific dependencies in ovarian cancer. Proc. Natl. Acad. Sci. USA *108*, 12372–12377.

Chin, L., Tam, A., Pomerantz, J., Wong, M., Holash, J., Bardeesy, N., Shen, Q., O'Hagan, R., Pantginis, J., Zhou, H., et al. (1999). Essential role for oncogenic Ras in tumour maintenance. Nature *400*, 468–472.

Chng, W.J., Huang, G.F., Chung, T.H., Ng, S.B., Gonzalez-Paz, N., Troska-Price, T., Mulligan, G., Chesi, M., Bergsagel, P.L., and Fonseca, R. (2011). Clinical and biological implications of MYC activation: a common difference between MGUS and newly diagnosed multiple myeloma. Leukemia *25*, 1026–1035.

Claudio, J.O., Masih-Khan, E., Tang, H., Gonçalves, J., Voralia, M., Li, Z.H., Nadeem, V., Cukerman, E., Francisco-Pabalan, O., Liew, C.C., et al. (2002). A molecular compendium of genes expressed in multiple myeloma. Blood *100*, 2175–2186.

Cole, P.A. (2008). Chemical probes for histone-modifying enzymes. Nat. Chem. Biol. *4*, 590–597.

Conaway, R.C., and Conaway, J.W. (2011). Function and regulation of the Mediator complex. Curr. Opin. Genet. Dev. *21*, 225–230.

Creyghton, M.P., Cheng, A.W., Welstead, G.G., Kooistra, T., Carey, B.W., Steine, E.J., Hanna, J., Lodato, M.A., Frampton, G.M., Sharp, P.A., et al. (2010). Histone H3K27ac separates active from poised enhancers and predicts developmental state. Proc. Natl. Acad. Sci. USA *107*, 21931–21936.

Dawson, M.A., and Kouzarides, T. (2012). Cancer epigenetics: from mechanism to therapy. Cell *150*, 12–27.

Dawson, M.A., Prinjha, R.K., Dittmann, A., Giotopoulos, G., Bantscheff, M., Chan, W.I., Robson, S.C., Chung, C.W., Hopf, C., Savitski, M.M., et al. (2011). Inhibition of BET recruitment to chromatin as an effective treatment for MLL-fusion leukaemia. Nature *478*, 529–533.

Delmore, J.E., Issa, G.C., Lemieux, M.E., Rahl, P.B., Shi, J., Jacobs, H.M., Kastritis, E., Gilpatrick, T., Paranal, R.M., Qi, J., et al. (2011). BET bromodomain inhibition as a therapeutic strategy to target c-Myc. Cell *146*, 904–917.

Dey, A., Chitsaz, F., Abbasi, A., Misteli, T., and Ozato, K. (2003). The double bromodomain protein Brd4 binds to acetylated chromatin during interphase and mitosis. Proc. Natl. Acad. Sci. USA *100*, 8758–8763.

Dib, A., Gabrea, A., Glebov, O.K., Bergsagel, P.L., and Kuehl, W.M. (2008). Characterization of MYC translocations in multiple myeloma cell lines. J. Natl. Cancer Inst. Monogr. *39*, 25–31.

Dixon, J.R., Selvaraj, S., Yue, F., Kim, A., Li, Y., Shen, Y., Hu, M., Liu, J.S., and Ren, B. (2012). Topological domains in mammalian genomes identified by analysis of chromatin interactions. Nature *485*, 376–380.

Elsässer, S.J., Allis, C.D., and Lewis, P.W. (2011). Cancer. New epigenetic drivers of cancers. Science *331*, 1145–1146.

Esteller, M. (2008). Epigenetics in cancer. N. Engl. J. Med. *358*, 1148–1159.

Feinberg, A.P., and Tycko, B. (2004). The history of cancer epigenetics. Nat. Rev. Cancer *4*, 143–153.

Felsher, D.W., and Bishop, J.M. (1999). Reversible tumorigenesis by MYC in hematopoietic lineages. Mol. Cell *4*, 199–207.

Filippakopoulos, P., Qi, J., Picaud, S., Shen, Y., Smith, W.B., Fedorov, O., Morse, E.M., Keates, T., Hickman, T.T., Felletar, I., et al. (2010). Selective inhibition of BET bromodomains. Nature *468*, 1067–1073.

Garraway, L.A., and Sellers, W.R. (2006). Lineage dependency and lineage-survival oncogenes in human cancer. Nat. Rev. Cancer *6*, 593–602.

Garraway, L.A., Widlund, H.R., Rubin, M.A., Getz, G., Berger, A.J., Ramaswamy, S., Beroukhim, R., Milner, D.A., Granter, S.R., Du, J., et al. (2005).

Integrative genomic analyses identify MITF as a lineage survival oncogene amplified in malignant melanoma. Nature *436*, 117–122.

Geutjes, E.J., Bajpe, P.K., and Bernards, R. (2012). Targeting the epigenome for treatment of cancer. Oncogene *31*, 3827–3844.

Giese, K., Kingsley, C., Kirshner, J.R., and Grosschedl, R. (1995). Assembly and function of a TCR alpha enhancer complex is dependent on LEF-1-induced DNA bending and multiple protein-protein interactions. Genes Dev. *9*, 995–1008.

Giniger, E., and Ptashne, M. (1988). Cooperative DNA binding of the yeast transcriptional activator GAL4. Proc. Natl. Acad. Sci. USA *85*, 382–386.

Göndör, A., and Ohlsson, R. (2009). Chromosome crosstalk in three dimensions. Nature *461*, 212–217.

Griggs, D.W., and Johnston, M. (1991). Regulated expression of the GAL4 activator gene in yeast provides a sensitive genetic switch for glucose repression. Proc. Natl. Acad. Sci. USA *88*, 8597–8601.

Heintzman, N.D., Hon, G.C., Hawkins, R.D., Kheradpour, P., Stark, A., Harp, L.F., Ye, Z., Lee, L.K., Stuart, R.K., Ching, C.W., et al. (2009). Histone modifications at human enhancers reflect global cell-type-specific gene expression. Nature *459*, 108–112.

Holien, T., Våtsveen, T.K., Hella, H., Waage, A., and Sundan, A. (2012). Addiction to c-MYC in multiple myeloma. Blood *120*, 2450–2453.

Issa, J.P., and Kantarjian, H.M. (2009). Targeting DNA methylation. Clin. Cancer Res. *15*, 3938–3946.

Jain, M., Arvanitis, C., Chu, K., Dewey, W., Leonhardt, E., Trinh, M., Sundberg, C.D., Bishop, J.M., and Felsher, D.W. (2002). Sustained loss of a neoplastic phenotype by brief inactivation of MYC. Science *297*, 102–104.

Jang, M.K., Mochizuki, K., Zhou, M., Jeong, H.S., Brady, J.N., and Ozato, K. (2005). The bromodomain protein Brd4 is a positive regulatory component of P-TEFb and stimulates RNA polymerase II-dependent transcription. Mol. Cell *19*, 523–534.

Jiang, Y.W., Veschambre, P., Erdjument-Bromage, H., Tempst, P., Conaway, J.W., Conaway, R.C., and Kornberg, R.D. (1998). Mammalian mediator of transcriptional regulation and its possible role as an end-point of signal transduction pathways. Proc. Natl. Acad. Sci. USA *95*, 8538–8543.

Kagey, M.H., Newman, J.J., Bilodeau, S., Zhan, Y., Orlando, D.A., van Berkum, N.L., Ebmeier, C.C., Goossens, J., Rahl, P.B., Levine, S.S., et al. (2010). Mediator and cohesin connect gene expression and chromatin architecture. Nature *467*, 430–435.

Kim, T.K., and Maniatis, T. (1997). The mechanism of transcriptional synergy of an in vitro assembled interferon-beta enhanceosome. Mol. Cell *1*, 119–129.

Kornberg, R.D. (2005). Mediator and the mechanism of transcriptional activation. Trends Biochem. Sci. *30*, 235–239.

Krueger, B.J., Varzavand, K., Cooper, J.J., and Price, D.H. (2010). The mechanism of release of P-TEFb and HEXIM1 from the 7SK snRNP by viral and cellular activators includes a conformational change in 7SK. PLoS ONE *5*, e12335.

Langmead, B., Trapnell, C., Pop, M., and Salzberg, S.L. (2009). Ultrafast and memory-efficient alignment of short DNA sequences to the human genome. Genome Biol. *10*, R25.

Lelli, K.M., Slattery, M., and Mann, R.S. (2012). Disentangling the many layers of eukaryotic transcriptional regulation. Annu. Rev. Genet. *46*, 43–68.

LeRoy, G., Rickards, B., and Flint, S.J. (2008). The double bromodomain proteins Brd2 and Brd3 couple histone acetylation to transcription. Mol. Cell *30*, 51–60.

Lin, C.Y., Lovén, J., Rahl, P.B., Paranal, R.M., Burge, C.B., Bradner, J.E., Lee, T.I., and Young, R.A. (2012). Transcriptional amplification in tumor cells with elevated c-Myc. Cell *151*, 56–67.

Maldonado, V., and Melendez-Zajgla, J. (2011). Role of Bcl-3 in solid tumors. Mol. Cancer *10*, 152.

Malik, S., and Roeder, R.G. (2010). The metazoan Mediator co-activator complex as an integrative hub for transcriptional regulation. Nat. Rev. Genet. *11*, 761–772.

Marks, P.A., and Xu, W.S. (2009). Histone deacetylase inhibitors: Potential in cancer therapy. J. Cell. Biochem. *107*, 600–608.

Mertz, J.A., Conery, A.R., Bryant, B.M., Sandy, P., Balasubramanian, S., Mele, D.A., Bergeron, L., and Sims, R.J., 3rd. (2011). Targeting MYC dependence in cancer by inhibiting BET bromodomains. Proc. Natl. Acad. Sci. USA *108*, 16669–16674.

Musgrove, E.A., Caldon, C.E., Barraclough, J., Stone, A., and Sutherland, R.L. (2011). Cyclin D as a therapeutic target in cancer. Nat. Rev. Cancer *11*, 558–572.

Nicodeme, E., Jeffrey, K.L., Schaefer, U., Beinke, S., Dewell, S., Chung, C.W., Chandwani, R., Marazzi, I., Wilson, P., Coste, H., et al. (2010). Suppression of inflammation by a synthetic histone mimic. Nature *468*, 1119–1123.

Ong, C.T., and Corces, V.G. (2011). Enhancer function: new insights into the regulation of tissue-specific gene expression. Nat. Rev. Genet. *12*, 283–293.

Ott, C.J., Kopp, N., Bird, L., Paranal, R.M., Qi, J., Bowman, T., Rodig, S.J., Kung, A.L., Bradner, J.E., and Weinstock, D.M. (2012). BET bromodomain inhibition targets both c-Myc and IL7R in high-risk acute lymphoblastic leukemia. Blood *120*, 2843–2852.

Pedersen, N., Mortensen, S., Sørensen, S.B., Pedersen, M.W., Rieneck, K., Bovin, L.F., and Poulsen, H.S. (2003). Transcriptional gene expression profiling of small cell lung cancer cells. Cancer Res. *63*, 1943–1953.

Perk, J., Iavarone, A., and Benezra, R. (2005). Id family of helix-loop-helix proteins in cancer. Nat. Rev. Cancer *5*, 603–614.

Rada-Iglesias, A., Bajpai, R., Swigut, T., Brugmann, S.A., Flynn, R.A., and Wysocka, J. (2011). A unique chromatin signature uncovers early developmental enhancers in humans. Nature *470*, 279–283.

Rahman, S., Sowa, M.E., Ottinger, M., Smith, J.A., Shi, Y., Harper, J.W., and Howley, P.M. (2011). The Brd4 extraterminal domain confers transcription activation independent of pTEFb by recruiting multiple proteins, including NSD3. Mol. Cell. Biol. *31*, 2641–2652.

Reimold, A.M., Iwakoshi, N.N., Manis, J., Vallabhajosyula, P., Szomolanyi-Tsuda, E., Gravallese, E.M., Friend, D., Grusby, M.J., Alt, F., and Glimcher, L.H. (2001). Plasma cell differentiation requires the transcription factor XBP-1. Nature *412*, 300–307.

Shaffer, A.L., Emre, N.C., Lamy, L., Ngo, V.N., Wright, G., Xiao, W., Powell, J., Dave, S., Yu, X., Zhao, H., et al. (2008). IRF4 addiction in multiple myeloma. Nature *454*, 226–231.

Shah, N., Pang, B., Yeoh, K.G., Thorn, S., Chen, C.S., Lilly, M.B., and Salto-Tellez, M. (2008). Potential roles for the PIM1 kinase in human cancer - a molecular and therapeutic appraisal. Eur. J. Cancer *44*, 2144–2151.

Shapiro-Shelef, M., Lin, K.I., McHeyzer-Williams, L.J., Liao, J., McHeyzer-Williams, M.G., and Calame, K. (2003). Blimp-1 is required for the formation of immunoglobulin secreting plasma cells and pre-plasma memory B cells. Immunity *19*, 607–620.

Shou, Y., Martelli, M.L., Gabrea, A., Qi, Y., Brents, L.A., Roschke, A., Dewald, G., Kirsch, I.R., Bergsagel, P.L., and Kuehl, W.M. (2000). Diverse karyotypic abnormalities of the c-myc locus associated with c-myc dysregulation and tumor progression in multiple myeloma. Proc. Natl. Acad. Sci. USA *97*, 228–233.

Spitz, F., and Furlong, E.E. (2012). Transcription factors: from enhancer binding to developmental control. Nat. Rev. Genet. *13*, 613–626.

Taatjes, D.J. (2010). The human Mediator complex: a versatile, genome-wide regulator of transcription. Trends Biochem. Sci. *35*, 315–322.

Thanos, D., and Maniatis, T. (1995). Virus induction of human IFN beta gene expression requires the assembly of an enhanceosome. Cell *83*, 1091–1100.

Turner, C.A., Jr., Mack, D.H., and Davis, M.M. (1994). Blimp-1, a novel zinc finger-containing protein that can drive the maturation of B lymphocytes into immunoglobulin-secreting cells. Cell *77*, 297–306.

Weinstein, I.B. (2002). Cancer. Addiction to oncogenes—the Achilles heal of cancer. Science *297*, 63–64.

Whyte, W.A., Orlando, D.A., Hnisz, D., Abraham, B.J., Lin, C.Y., Kagey, M.H., Rahl, P.B., Lee, T.I., and Young, R.A. (2013). Master transcription factors and

mediator establish super-enhancers at key cell identity genes. Cell *153*, this issue, 307–319.

Wu, S.Y., and Chiang, C.M. (2007). The double bromodomain-containing chromatin adaptor Brd4 and transcriptional regulation. J. Biol. Chem. *282*, 13141–13145.

Wu, S.Y., Zhou, T., and Chiang, C.M. (2003). Human mediator enhances activator-facilitated recruitment of RNA polymerase II and promoter recognition by TATA-binding protein (TBP) independently of TBP-associated factors. Mol. Cell. Biol. *23*, 6229–6242.

Wu, S.Y., Lee, A.Y., Lai, H.T., Zhang, H., and Chiang, C.M. (2013). Phospho switch triggers brd4 chromatin binding and activator recruitment for gene-specific targeting. Mol. Cell *49*, 843–857.

Yang, Z., Yik, J.H., Chen, R., He, N., Jang, M.K., Ozato, K., and Zhou, Q. (2005). Recruitment of P-TEFb for stimulation of transcriptional elongation by the bromodomain protein Brd4. Mol. Cell *19*, 535–545.

You, J.S., and Jones, P.A. (2012). Cancer genetics and epigenetics: two sides of the same coin? Cancer Cell *22*, 9–20.

Zhang, Y., Liu, T., Meyer, C.A., Eeckhoute, J., Johnson, D.S., Bernstein, B.E., Nusbaum, C., Myers, R.M., Brown, M., Li, W., and Liu, X.S. (2008). Model-based analysis of ChIP-Seq (MACS). Genome Biol. *9*, R137.

Zhang, W., Prakash, C., Sum, C., Gong, Y., Li, Y., Kwok, J.J., Thiessen, N., Pettersson, S., Jones, S.J., Knapp, S., et al. (2012). Bromodomain-containing protein 4 (BRD4) regulates RNA polymerase II serine 2 phosphorylation in human CD4+ T cells. J. Biol. Chem. *287*, 43137–43155.

Zuber, J., Shi, J., Wang, E., Rappaport, A.R., Herrmann, H., Sison, E.A., Magoon, D., Qi, J., Blatt, K., Wunderlich, M., et al. (2011). RNAi screen identifies Brd4 as a therapeutic target in acute myeloid leukaemia. Nature *478*, 524–528.

EXTENDED EXPERIMENTAL PROCEDURES

Cell Culture

MM1.S MM cells (CRL-2974 ATCC) and U-87 MG glioblastoma cells (HTB-14 ATCC) were purchased from ATCC. H2171 small cell lung carcinoma cells (CRL-5929 ATCC) were kindly provided by John Minna, UT Southwestern. MM1.S and H2171 cells were propagated in RPMI-1640 supplemented with 10% fetal bovine serum and 1% GlutaMAX (Invitrogen, 35050-061). U-87 MG cells were cultured in Eagle's Minimum Essential Medium (EMEM) modified to contain Earles Balanced Salt Solution, nonessential amino acids, 2 mM L-glutamine, 1 mM sodium pyruvate, and 1,500 mg/l sodium bicarbonate. Cells were grown at 37°C and 5% CO_2.

JQ1 was kindly provided by James Bradner, Dana Farber Cancer Institute. For JQ1 dose dependence experiments, cells were resuspended in fresh media containing JQ1 (5 nM, 50 nM, 500 nM, 5,000 nM) or vehicle (DMSO, 0.05%) for a duration of 6 hr, unless otherwise indicated. For JQ1 time course experiments, cells were resuspended in fresh media containing 500 nM JQ1 and sampled at various time points.

Chromatin Immunoprecipitation

Cells were crosslinked for 10 min at room temperature by the addition of one-tenth of the volume of 11% formaldehyde solution (11% formaldehyde, 50 mM HEPES pH 7.3, 100 mM NaCl, 1 mM EDTA pH 8.0, 0.5 mM EGTA pH 8.0) to the growth media followed by 5 min quenching with 100 mM glycine. Cells were washed twice with PBS, then the supernatant was aspirated and the cell pellet was flash frozen in liquid nitrogen. Frozen crosslinked cells were stored at −80°C. 100ul of Dynal magnetic beads (Sigma) were blocked with 0.5% BSA (w/v) in PBS. Magnetic beads were bound with 10 μg of the indicated antibody.

For BRD4 occupied genomic regions, we performed ChIP-Seq experiments using a Bethyl Laboratories (A301-985A, lot A301-985A-1) antibody. The affinity purified antibody was raised in rabbit against an epitope corresponding to amino acids 1312-1362 of human BRD4. Antibody specificity was previously determined (Dawson et al., 2011). For MED1 (CRSP1/TRAP220) occupied genomic regions, we performed ChIP-Seq experiments using a Bethyl Laboratories (A300-793A, lot A300-783A) antibody. The affinity purified antibody was raised in rabbit against an epitope corresponding to amino acids 1523-1581 mapping at the C terminus of human MED1. For CDK9 occupied genomic regions, we performed ChIP-Seq experiments using a Santa Cruz Biotechnology (sc-484, lot D1612) antibody. For RNA polymerase II occupied genomic regions, we performed ChIP-Seq experiments using a Santa Cruz Biotechnology (sc-899, lot K0111) antibody. The affinity purified antibody was raised in rabbit against an epitope mapping to the N-terminus of murine RBP1, the largest subunit of RNA Pol II.

For MM1.S, crosslinked cells were lysed with lysis buffer 1 (50 mM HEPES pH 7.3, 140 mM NaCl, 1 mM EDTA, 10% glycerol, 0.5% NP-40, and 0.25% Triton X-100) and resuspended and sonicated in sonication buffer (20 mM Tris-HCl pH 8.0, 150 mM NaCl, 2 mM EDTA pH 8.0, 0.1% SDS, and 1% Triton X-100). Cells were sonicated for 10 cycles at 30 s each on ice (18-21 W) with 60 s on ice between cycles. Sonicated lysates were cleared and incubated overnight at 4°C with magnetic beads bound with antibody to enrich for DNA fragments bound by the indicated factor. Beads were washed two times with sonication buffer, one time with sonication buffer with 500 mM NaCl, one time with LiCl wash buffer (10 mM Tris pH 8.0, 1 mM EDTA, 250 mM LiCl, 1% NP-40,) and one time with TE with 50 mMNaCl. DNA was eluted in elution buffer (50 mM Tris-HCL pH 8.0, 10 mM EDTA, 1% SDS). Cross-links were reversed overnight. RNA and protein were digested using RNase A and Proteinase K, respectively and DNA was purified with phenol chloroform extraction and ethanol precipitation.

For BRD4 ChIPs in U-87 MG and H2171, crosslinked cells were lysed with lysis buffer 1 (50 mM HEPES [pH 7.3], 140 mM NaCl, 1 mM EDTA, 10% glycerol, 0.5% NP-40, and 0.25% Triton X-100) and washed with lysis buffer 2 (10 mM Tris-HCl [pH 8.0], 200 mM NaCl, 1 mM EDTA [pH 8.0] and 0.5 mM EGTA [pH 8.0]). Cells were resuspended and sonicated in sonication buffer (50 mM Tris-HCl [pH 7.5], 140 mM NaCl, 1 mM EDTA, 1 mM EGTA, 1% Triton X-100, 0.1% SDS) for nine cycles at 30 s each on ice (18–21 W) with 60 s on ice between cycles. Sonicated lysates were cleared and incubated overnight at 4°C with magnetic beads bound with antibody to enrich for DNA fragments bound by the indicated factor. Beads were washed three times with sonication buffer, one time with sonication buffer with 500 mM NaCl, one time with LiCl wash buffer (20 mM Tris [pH 8.0], 1 mM EDTA, 250 mM LiCl, 0.5% NP-40, 0.5% Na-deoxycholate) and one time with TE. DNA was eluted in elution buffer. Crosslinks were reversed overnight. RNA and protein were digested using RNase A and Proteinase K, respectively and DNA was purified with phenol chloroform extraction and ethanol precipitation.

ChIP-Seq data sets of H3K4Me3 and H3K27Ac in MM1.S, and MED1 and H3K27Ac in U-87 MG and H2171 were previously published (Lin et al., 2012).

Illumina Sequencing and Library Generation

Purified ChIP DNA was used to prepare Illumina multiplexed sequencing libraries. Libraries for Illumina sequencing were prepared following the Illumina TruSeq DNA Sample Preparation v2 kit protocol with the following exceptions. After end-repair and A-tailing, Immunoprecipitated DNA (~10-50 ng) or Whole Cell Extract DNA (50 ng) was ligated to a 1:50 dilution of Illumina Adaptor Oligo Mix assigning one of 24 unique indexes in the kit to each sample. Following ligation, libraries were amplified by 18 cycles of PCR using the HiFi NGS Library Amplification kit from KAPA Biosystems. Amplified libraries were then size-selected using a 2% gel cassette in the Pippin Prep system from Sage Science set to capture fragments between 200 and 400 bp. Libraries were

quantified by qPCR using the KAPA Biosystems Illumina Library Quantification kit according to kit protocols. Libraries with distinct TruSeq indexes were multiplexed by mixing at equimolar ratios and running together in a lane on the Illumina HiSeq 2000 for 40 bases in single read mode.

Luciferase Reporter Assays

A minimal Myc promoter was amplified from human genomic DNA and cloned into the SacI and HindIII sites of the pGL3 basic vector (Promega). Enhancer fragments were likewise amplified from human genomic DNA and cloned into the BamHI and SalI sites of the pGL3-pMyc vector. All cloning primers are listed in Table S6. Constructs were transfected into MM1.S cells using Lipofectamine 2000 (Invitrogen). The pRL-SV40 plasmid (Promega) was cotransfected as a normalization control. Cells were incubated for 24 hr, and luciferase activity was measured using the Dual-Luciferase Reporter Assay System (Promega). For the JQ1 concentration course, cells were resuspended in fresh media containing various concentrations of JQ1 24 hr after transfection, and incubated for an additional 6 hr before harvesting. Luminescence measurements were made using the Dual-Luciferase Reporter Assay System (Promega) on a Wallac EnVision (Perkin Elmer) plate reader.

Cell Viability Assays

Cell viability was measured using the CellTiterGlo Assay kit (Promega, G7571). MM1.S cells were resuspended in fresh media containing JQ1 (5 nM, 50 nM, 500 nM, 5,000 nM) or vehicle (DMSO, 0.05%), then plated in 96-well plates at 10,000 cells/well in a volume of 100uL. Viability was measured after 6, 24, 48 and 72 hr incubations by addition of CellTiter Glo reagent and luminescence measurement on a Tecan Safire^2 plate reader.

Western Blotting

Total cell lysates for immunoblotting were prepared by pelleting 1x10^6 cells from each cell line at 4°C (1,200 rpm) for 5 min using a Sorvall Legend centrifuge (Thermo Fisher Scientific). After collecting the cells the pellets were washed 1X with ice-cold 1X PBS and the pellet after the final wash was resuspended in RIPA lysis buffer (Sigma, R0278) containing 150 mM NaCl, 1.0% IGEPAL CA-630, 0.5% sodium deoxycholate, 0.1% SDS, 50 mM Tris [pH 8.0], 2X Halt Protease inhibitors (Pierce, Thermo Fisher Scientific), and 2X Phosphatase inhibitor cocktail 2 (Sigma, P5726) and 3 (Sigma, P0044). Total protein lysates were collected and snap-frozen in liquid nitrogen before being stored at −80°C. Protein concentrations were determined by using the Bradford protein assay (Bio-Rad, #500-0006). Total cell lysates were loaded per well onto NuPAGE NOVEX 4%–12% Bis-Tris Mini Gel (Invitrogen, Carlsbad, CA) and separated by electrophoreses at 200 V for 1 hr. The gels were then transferred onto a PVDF membrane (Immobilon-P; Millipore, Billerica, MA) by semi-dry transfer system (TransBlot SD; Bio-Rad) and blocked by incubation with 5% dry milk in TBST (TBS with 0.2% Tween-20). Membranes were probed using antibodies raised against c-Myc (Epitomics, category: 1472-1), BRD4 (Epitomics, category: 5716-1) or β-Actin (Sigma, clone AC-15, A5441). Chemiluminescent detection was performed with appropriate secondary antibodies and developed using high-resolution BioMax MR film (Kodak, category: 870 13012).

RNA Extraction and Synthetic RNA Spike-In

Total RNA and sample preparation was preformed as previously described (Lovén et al., 2012). Briefly, MM1.S cells were incubated in JQ1-containing media (5 nM, 50 nM, 500 nM, 5,000 nM) or vehicle (DMSO, 0.05%) for a duration of 6 hr. Cell numbers were determined by manually counting cells using C-Chip disposable hemocytometers (Digital Bio, DHC-N01) prior to lysis and RNA extraction. Biological duplicates (equivalent to ten million cells per replicate) were subsequently collected and homogenized in 1 ml of TRIzol Reagent (Life Technologies, 15596-026), purified using the mirVANA miRNA isolation kit (Ambion, AM1560) following the manufacturer's instructions and re-suspended in 100 μl nuclease-free water (Ambion, AM9938). Total RNA was spiked-in with ERCC RNA Spike-In Mix (Ambion, 4456740), treated with DNA-*free*TM DNase I (Ambion, AM1906) and analyzed on Agilent 2100 Bioanalyzer for integrity. RNA with the RNA Integrity Number (RIN) above 9.8 was hybridized to GeneChip PrimeView Human Gene Expression Arrays (Affymetrix).

Microarray Sample Preparation and Analysis

For microarray analysis, 100 ng of total RNA containing ERCC RNA Spike-In Mix (see above) was used to prepare biotinylated aRNA (cRNA) according to the manufacturer's protocol (3′ IVT Express Kit, Affymetrix 901228). GeneChip arrays (Primeview, Affymetrix 901837) were hybridized and scanned according to standard Affymetrix protocols. All samples were processed in technical duplicate. Images were extracted with Affymetrix GeneChip Command Console (AGCC), and analyzed using GeneChip Expression Console. A Primeview CDF that included probe information for the ERCC controls, provided by Affymetrix, was used to generate .CEL files. We processed the CEL files using standard tools available within the *affy* package in R. The CEL files were processed with the *expresso* command to convert the raw probe intensities to probeset expression values. The parameters of the expresso command were set to generate Affymetrix MAS5-normalized probeset values. We used a loess regression to re-normalize these MAS5 normalized probeset values, using only the spike-in probesets to fit the loess. The *affy* package provides a function, *loess.normalize*, which will perform loess regression on a matrix of values (defined using the parameter *mat)* and allows for the user to specify which subset of data to use when fitting the loess (defined using the parameter *subset*, see the *affy* package documentation for further details*)*. For this application the parameters *mat* and *subset* were set as the

MAS5-normalized values and the row-indices of the ERCC control probesets, respectively. The default settings for all other parameters were used. The result of this was a matrix of expression values normalized to the control ERCC probes. The probeset values from the duplicates were averaged together and the Log_2 fold change comparing the control to the JQ1 treated samples are shown. Spike-in normalized gene expression tables can be found online associated with the GEO Accession ID GSE44929 (www.ncbi.nlm.nih.gov/geo/).

Data Analysis

Accessing Data Generated in This Manuscript

All ChIP-Seq and expression data generated in this manuscript can be found online associated with GEO Accession ID GSE44931 (www.ncbi.nlm.nih.gov/geo/).

Gene Sets and Annotations

All analysis was performed using RefSeq (NCBI36/HG18) (Pruitt et al., 2007) human gene annotations.

BRD4 Expression in Human Tissues

Processed gene expression values for 90 distinct normal tissues were retrieved from the Human Body Index (GSE7307). *BRD4* expression values were calculated by averaging expression values for three distinct probes that aligned to the sense strand of the *BRD4* transcript. Since in any given tissue, approximately 50% of all genes are expressed (Ramsköld et al., 2009), we classified *BRD4* as expressed in a given tissue if the average expression values of its probes was greater than the median expressed probe in the respective tissue. Using this metric, *BRD4* was determined to be expressed in 95% of all human tissues.

ChIP-Seq Data Processing

All ChIP-Seq data sets were aligned using Bowtie (version 0.12.9) (Langmead et al., 2009) to build version NCBI36/HG18 of the human genome. Alignments were performed using the following criteria: -n2, -e70, -m1, -k1,–best. These criteria preserved only reads that mapped uniquely to the genome with 1 or fewer mismatches. Aligned and raw data can be found online associated with the GEO Accession ID GSE42355 (www.ncbi.nlm.nih.gov/geo/).

Calculating Read Density

We developed a simple method to calculate the normalized read density of a ChIP-Seq data set in any region (Lin et al., 2012). ChIP-Seq reads aligning to the region were extended by 200bp and the density of reads per basepair (bp) was calculated. In order to eliminate PCR bias, multiple reads of the exact same sequence aligning to a single position were collapsed into a single read. Only positions with at least 2 overlapping extended reads contributed to the overall region density. The density of reads in each region was normalized to the total number of million mapped reads producing read density in units of reads per million mapped reads per bp (rpm/bp).

Identifying ChIP-Seq-Enriched Regions

We used the MACS version 1.4.2 (Model based analysis of ChIP-Seq) (Zhang et al., 2008) peak finding algorithm to identify regions of ChIP-Seq enrichment over background. A p value threshold of enrichment of 1e-9 was used for all data sets. The GEO accession number and background used for each data set can be found in the accompanying supplemental file (Table S6).

Defining Actively Transcribed Genes

In MM1.S and U-87 MG cells, a gene was defined as actively transcribed if enriched regions for H3K4me3, RNA Polymerase II (RNA Pol II), BRD4, and Mediator were located within ± 5kb of the TSS. In H2171 cells, a gene was defined as actively transcribed if enriched regions for H3K4me3, RNA Polymerase II (RNA Pol II), and BRD4,were located within ± 5kb of the TSS. Mediator was omitted in H2171 transcribed gene definitions due to the lower numbers of enriched regions for the factor. H3K4me3 is a histone modification associated with transcription initiation (Guenther et al., 2007) and BRD4 and Mediator have been shown to also occupy promoters of active genes (Kagey et al., 2010; Zhang et al., 2012). Using these criteria, we identified transcriptionally active genes in MM1.S, U-87 MG, and H2171 cells (Table S1).

Defining Active Enhancers

Active enhancers form loops with promoters that are facilitated by the Mediator complex (Kagey et al., 2010), thus we used regions of ChIP-Seq enrichment for the Mediator complex component MED1 outside of promoters (e.g., a region not contained within ± 2.5kb region flanking the promoter) to define active enhancers. In order to accurately capture dense clusters of enhancers, we allowed MED1 regions within 12.5kb of one another to be stitched together (see Whyte et al., 2013). We noticed that in some cases stitched regions in gene dense areas spanned multiple transcriptionally active genes and were likely not representative of enhancer clusters. Thus, stitched regions spanning more than two promoters of active genes were excluded from the analysis. This analysis defined enhancer regions in the MM1.S genome (Table S2). The same method was used to identify enhancers in the glioblastoma multiforme cell line U-87 MG and in the small cell lung cancer cell line H2171 (Table S4). Data S1 contains hg18 genome coordinate tracks for all enhancers in all profiled cell types in the form of a UCSC genome browser .bed file that can be uploaded and viewed at genome.ucsc.edu (Data S1).

Creating Meta Representations of ChIP-Seq Occupancy at Active Enhancers and Promoters

Genome-wide average "meta" representations of ChIP-Seq occupancy at active enhancers and promoters were created by mapping ChIP-Seq read density to the 5kb regions flanking the center of active enhancer regions or transcription start sites (TSS) of active genes. Each active enhancer or TSS region was split into one hundred 50bp bins. All active enhancer or TSS regions were then aligned and the average background subtracted ChIP-Seq factor density in each bin was calculated to create a meta genome-wide average in units of rpm/bp. See Figures 1B, 4D, S3E, S4A, and S4B.

Correlating BRD4 and MED1 Occupancy with RNA Pol II at Promoters

All genes were ranked by increasing density of RNA Pol II ChIP-Seq reads in the promoter region (± 1kb of transcription start site (TSS) and binned in increments of 100 genes. The median ChIP-Seq density for promoter regions within each bin was calculated in rpm/bp for both RNA Pol II and BRD4 and plotted (BRD4) or shaded by binding density (RNA Pol II). The same method was applied for MED1 in place of BRD4. See Figure 1C.

Defining Promoter Boundaries in MM1.S Cells

Promoter regions are typically defined as the ± several kb region centered on the TSS. In order to produce a more accurate and gene specific definition of promoters, we used the promoter centric H3K4Me3 histone modification mark to delineate the span of promoters for actively transcribed genes in MM1.S. At these genes, the boundaries of the directly overlapping H3K4Me3 ChIP-Seq enriched region were used to define the upstream/downstream ends of the promoter.

Calculating Total ChIP-Seq Occupancy Signal at Enhancers and Promoters

The total ChIP-Seq occupancy signal at enhancers was calculated by first determining the average ChIP-Seq read density in the entire enhancer region (rpm/bp). This value was multiplied by the length of the region to produce total ChIP-Seq occupancy in units of total rpm. See Figures 2A, 7A, 7B, and S2A. For all cell lines used in this study the total MED1 ChIP-Seq occupancy signal at enhancers can be found in Table S2 (MM1.S) or Table S4 (GBM and SCLC).

The total ChIP-Seq occupancy signal at promoters was calculated similarly. In order to accurately compare signal at promoters to that at enhancers, promoters that overlapped super-enhancers were excluded from analysis (Figure S2A).

Correlations of total BRD4 and MED1 occupancy signal at enhancers and promoters were calculated using a Pearson correlation statistic (Figures S1A and S1B).

Identifying Super-Enhancers

We observed disproportionately high occupancy of factors such as MED1 and BRD4 at a subset of enhancers that we termed ''super-enhancers.'' To formally identify super-enhancers, we first ranked all enhancers by increasing total background subtracted ChIP-Seq occupancy of MED1 (x axis), and plotted the total background subtracted ChIP-Seq occupancy of MED1 in units of total rpm (y axis). This representation revealed a clear inflection point in the distribution of MED1 at enhancers (Figures 2A, 7A, and 7D). We geometrically defined the inflection point and used it to establish the cut off for super-enhancers. Enhancers that were classified as super-enhancers are noted in Table S2 (MM1.S) and Table S4 (GBM and SCLC).

Creating Metarepresentations of ChIP-Seq Occupancy at Typical Enhancers and Super-Enhancers

Genome-wide average ''meta'' representations of MED1 and BRD4 ChIP-Seq occupancy at typical enhancers and super-enhancers were created by mapping MED1 and BRD4 ChIP-Seq read density to the enhancer regions and their corresponding ± 5kb flanking regions. Each enhancer region was split into 100 equally sized bins. The flanking ± 5kb regions were split into 50bp bins. This split all enhancer regions, regardless of their size, into 300 bins. All typical enhancer or super-enhancer regions were then aligned and the average MED1 and BRD4 ChIP-Seq density in each bin was calculated to create a meta genome-wide average in units of rpm/bp. In order to visualize the length disparity between typical and super-enhancer regions, the enhancer region (between its actual start and end) was scaled relative to its average length. See Figure 2B (MM1.S), Figure 7B (GBM) and 7E (SCLC).

Characterizing Super-Enhancers

We calculated the total ChIP-Seq occupancy for MED1, BRD4, and H3K27Ac at super-enhancers and typical enhancers and determined the fold difference between the average signal at super-enhancers versus typical enhancers. ChIP-Seq density for MED1, BRD4, and H3K27Ac were determined by calculating the average density of each factor in constituent regions of every enhancer. See Figure 2B (MM1.S), Figure 7B (GBM) and 7E (SCLC).

Assigning Genes to Super-Enhancers

Transcriptionally active genes were assigned to enhancers using the following method: Enhancers tend to loop to and associate with adjacent genes in order to activate their transcription (Ong and Corces, 2011). Most of these interactions occur within a distance of ~50kb of the enhancer (Chepelev et al., 2012). Using a simple proximity rule, we assigned all transcriptionally active genes (TSSs) to super-enhancers within a 50kb window, a method shown to identify a large proportion of true enhancer/promoter interactions in embryonic stem cells (Dixon et al., 2012). This identified 681 genes associated with super-enhancers in MM1.S cells (Table S3). The same method was applied to identify super-enhancer-associated genes in GBM and SCLC (Table S5).

Calculating the Cell-Type Specificity of Enhancer-Associated Genes

Spike-in normalized gene expression levels for all genes in MM1.S cells were determined as previously described (RNA Extraction and Synthetic RNA Spike-In and Microarray Sample Preparation and Analysis sections). The expression levels of genes associated with typical enhancers or super-enhancers were compared using a Welch's t test and found be statistically significant (p value < 2e-16) (Figure 2D).

To evaluate the cell-type specificity of SE and typical enhancer -associated genes, we compared MM1.S gene expression from the data set (GSE17385) (Carrasco et al., 2007) to the largest matched microarray expression data set of normal human tissues (GSE7307) on Affymetrix U133 plus 2.0 arrays from Gene Expression Omnibus (GEO). We used the three positive controls from GSE17385 and the 504 samples of normal human tissues from GSE7307 for the analysis. All .CEL files were MAS5 normalized together and probe level intensities were reported using standard Affymetrix CDF. We used the entropy-based measure JS divergence to quantify cell-type specificity (Cabili et al., 2011). For each triplicate of MM1.S expression data set from GSE7307, the JS divergence quantified the similarity between a probe's expression pattern across the MM1.S data set and the 504 samples of normal

human tissues and a pre-defined pattern that represents an extreme case in which the probe is expressed only in MM1.S. The JS divergence statistic was converted to a Z-score to give a relative measure of the cell type specificity of genes in MM1.S compared to the average gene. A similar comparison of cell type specificity Z-scores also showed a statistically significant difference between genes associated with typical or super-enhancers (p value = 1e-14) (Figure 2D).

Quantifying Effects of JQ1 Treatment on BRD4 Occupancy Genome Wide

In order to quantify the effects of JQ1 treatment on the genomic occupancy of BRD4, we first calculated average BRD4 occupancy (in units of rpm/bp) at BRD4 enriched regions in DMSO treated cells. We next calculated the average BRD4 occupancy in those same regions in cells treated with 500 nM JQ1 for 6 hr. The distributions of BRD4 at enriched regions are plotted (Figure 4B). The difference in the distributions of BRD4 was compared using a Welch's t test and found to be statistically significant (p value < 1e-16) (Figure 4B).

Quantifying Effects of JQ1 Treatment on BRD4 Occupancy at Active Enhancers

In order to quantify the effects of JQ1 treatment on the genomic occupancy of BRD4 at active enhancers, we first calculated the BRD4 occupancy at typical enhancers or super-enhancers in DMSO and various concentrations of JQ1. The loss of BRD4 at typical enhancers or super-enhancers was quantified as the fraction of BRD4 occupancy remaining compared to DMSO. The average loss of BRD4 at typical enhancers and super-enhancers is plotted for DMSO and 5 nM, 50 nM, 500 nM JQ1 treatment in Figure 5F. 95% confidence intervals were determined by performing 10,000 random samplings (with replacement) of either super-enhancers or typical enhancers. Sample sizes were identical between typical enhancers and super-enhancers. The differences in the mean loss of BRD4 between typical enhancers and super-enhancers were also deemed significant (p value < 1e-8) at 5 nM, 50 nM, and 500 nM JQ1 treatment (Figure 5F) using a Welch's t test.

Quantifying Effects of JQ1 Treatment on Gene Expression in MM1.S

Spike-in normalized gene expression levels for all genes were determined as previously described (RNA Extraction and Synthetic RNA Spike-In and Microarray Sample Preparation and Analysis sections). In order to quantify changes in gene expression as a function of JQ1 treatment in a time or dose dependent manner, expression levels were first calculated for either super-enhancer or typical enhancer-associated genes (Figures 6B and 6C). For time dependent changes, the Log_2 fold change in expression was calculated relative to untreated control cells. For dose dependent changes, the Log_2 fold change in expression was calculated relative to DMSO treated cells. The average change in gene expression at super-enhancer or typical enhancer-associated genes was calculated at each time point or dose. In order to determine the significance of changes in the mean between super-enhancer and typical enhancer-associated genes, 95% confidence intervals were determined by performing 10,000 random samplings (with replacement) of the mean change for each set of genes. Sample sizes were identical between typical enhancer and super-enhancer-associated genes. We also determined the significance of the difference between distributions of gene expression values for super-enhancer and typical enhancer –associated genes at each time point or dose. Changes were significant over time at 3 and 6 hr after 500 nM JQ1 treatment (p value < 1e-8, Figure 6B). Changes were significant after 6 hr JQ1 treatments at doses of 50 nM, 500 nM, and 5,000 nM (p value < 1e-8, Figure 6C). Identical analysis was performed comparing changes in gene expression between super-enhancer-associated genes with multiple typical enhancers (Figures S3C and S3D). Changes were significant over time at 6 hr after 500 nM JQ1 treatment (p value = 0.03, Figure S3C). Changes were significant after 6 hr JQ1 treatments at a dose of 500 nM (p value = 0.052, Figure S3D).

Quantifying Effects of JQ1 Treatment on CDK9 and MED1 Occupancy at Promoters and Enhancers

We quantified changes in CDK9 and MED1 occupancy by calculating changes in CDK9 and MED1 ChIP-Seq occupancy at promoters, typical enhancers, and super-enhancers. Since super-enhancers often contain TSS overlapping regions, we used H3K4Me3 promoter definitions (Figure S2B) to exclude TSS overlapping super-enhancers. The change in CDK9 and MED1 occupancy was quantified as the fraction of factor occupancy remaining after 500 nM JQ1 treatment for 6 hr compared to DMSO. The average change in CDK9 and MED1 at promoters, typical enhancers, and super-enhancers is plotted in Figure 6F. To show the significance of changes in the mean, 95% confidence intervals were determined by performing 10,000 random samplings (with replacement) of the mean change at either super-enhancers or typical enhancers.

In order to determine the changes in CDK9 and MED1 occupancy at TSS overlapping and TSS distal portions of super-enhancers, we split super-enhancers into TSS proximal and TSS distal regions (Figure S3F). The average change in CDK9 and MED1 at super-enhancer TSS proximal and TSS distal regions is plotted in Figure S3F. To show the significance of changes in the mean, 95% confidence intervals were determined by performing 10,000 random samplings (with replacement) of the mean change at either super-enhancers or typical enhancers.

Quantifying Effects of JQ1 Treatment on Transcription Elongation

We quantified the effects of JQ1 treatment on transcription elongation of genes by measuring the change in RNA Pol II density in the elongating gene body region of genes. The elongating region of genes was defined as the region beginning 300bp downstream of the TSS and extending 3,000 bp past the annotated 3′ end of the transcript. RNA Pol II density (rpm/bp) was calculated in this region for all transcribed genes in cells treated with DMSO or 500 nM JQ1. The Log_2 fold change in RNA Pol II density ± 500 nM JQ1 treatment was calculated for all actively transcribed genes (Figure 6G).

To quantify the effects of JQ1 treatment on RNA Pol II elongation at typical or super-enhancer-associated genes, the Log_2 fold change in RNA Pol II density ± 500 nM JQ1 treatment was calculated for typical enhancer or super-enhancer-associated genes. The distributions of changes in RNA Pol II occupancy were statistically different as determined by a two sample Kolmogorov-Smirnov (KS) test (Figure S3G, p value < 2e-16). The average change in RNA Pol II between the two groups of genes was also examined

(Figure 6H) and the significance of change was shown using plotted 95% confidence intervals determined by performing 10,000 random samplings (with replacement) of the mean change for either super-enhancer or typical enhancer-associated genes.

SUPPLEMENTAL REFERENCES

Cabili, M.N., Trapnell, C., Goff, L., Koziol, M., Tazon-Vega, B., Regev, A., and Rinn, J.L. (2011). Integrative annotation of human large intergenic noncoding RNAs reveals global properties and specific subclasses. Genes Dev. *25*, 1915–1927.

Futreal, P.A., Coin, L., Marshall, M., Down, T., Hubbard, T., Wooster, R., Rahman, N., and Stratton, M.R. (2004). A census of human cancer genes. Nat. Rev. Cancer *4*, 177–183.

Guenther, M.G., Levine, S.S., Boyer, L.A., Jaenisch, R., and Young, R.A. (2007). A chromatin landmark and transcription initiation at most promoters in human cells. Cell *130*, 77–88.

Lovén, J., Orlando, D.A., Sigova, A.A., Lin, C.Y., Rahl, P.B., Burge, C.B., Levens, D.L., Lee, T.I., and Young, R.A. (2012). Revisiting global gene expression analysis. Cell *151*, 476–482.

Patel, M.N., Halling-Brown, M.D., Tym, J.E., Workman, P., and Al-Lazikani, B. (2013). Objective assessment of cancer genes for drug discovery. Nat. Rev. Drug Discov. *12*, 35–50.

Pruitt, K.D., Tatusova, T., and Maglott, D.R. (2007). NCBI reference sequences (RefSeq): a curated non-redundant sequence database of genomes, transcripts and proteins. Nucleic Acids Res. *35*(Database issue), D61–D65.

Ramsköld, D., Wang, E.T., Burge, C.B., and Sandberg, R. (2009). An abundance of ubiquitously expressed genes revealed by tissue transcriptome sequence data. PLoS Comput. Biol. *5*, e1000598.

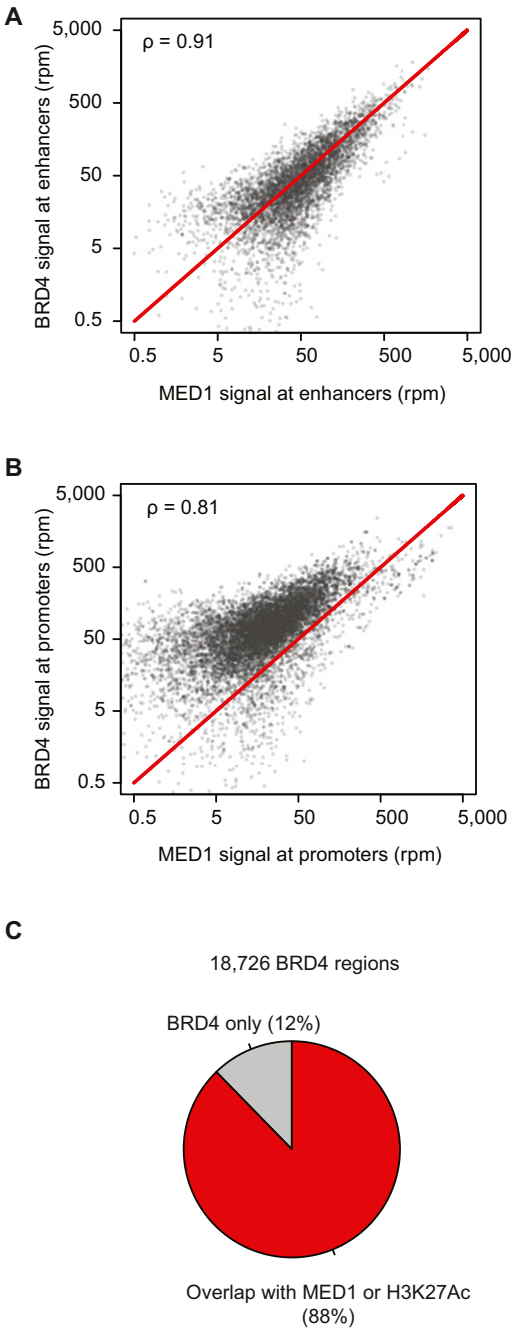

Figure S1. Mediator and BRD4 Co-occupy Promoters of Active Genes in Multiple Myeloma, Related to Figure 1

(A) Scatter plots showing the relationship between MED1 (x axis) and BRD4 (y axis) ChIP-Seq occupancy at individual enhancers in MM1.S cells. Units are in total ChIP-Seq reads per million in enhancer regions. The Pearson correlation score between MED1 and BRD4 is displayed (ρ = 0.91).

(B) Scatter plots showing the relationship between MED1 (x axis) and BRD4 (y axis) ChIP-Seq occupancy at individual promoters of actively transcribed genes in MM1.S cells. Units are in total ChIP-Seq reads per million in enhancer regions. The Pearson correlation score between MED1 and BRD4 is displayed (ρ = 0.81).

(C) Pie chart showing the overlap of BRD4 regions with either MED1 or H3K27Ac regions. BRD4 regions that overlap either a MED1 or H3K27Ac enriched region are shaded in red. BRD4 regions without any overlap are shaded in gray.

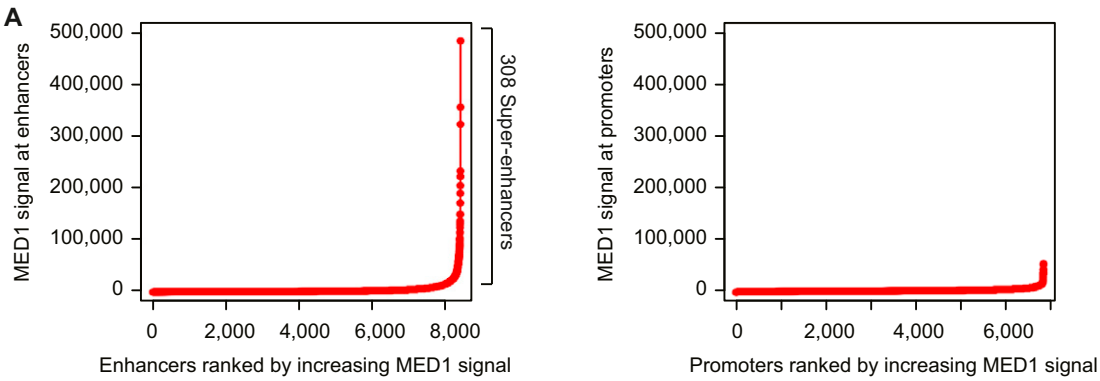

Figure S2. Super-Enhancers Identified in Multiple Myeloma, Related to Figure 2

(A) Left: Total MED1 ChIP-Seq signal in units of reads per million in enhancer regions for all enhancers in MM1.S. Enhancers are ranked by increasing MED1 ChIP-Seq signal. Right: Total MED1 ChIP-Seq signal in units of reads per million in promoter regions for all promoters of actively transcribed genes in MM1.S that do not overlap with a super-enhancer. Promoters are ranked by increasing MED1 ChIP-Seq signal. In both plots, y axis shows MED1 signal from 0 to 500,000.

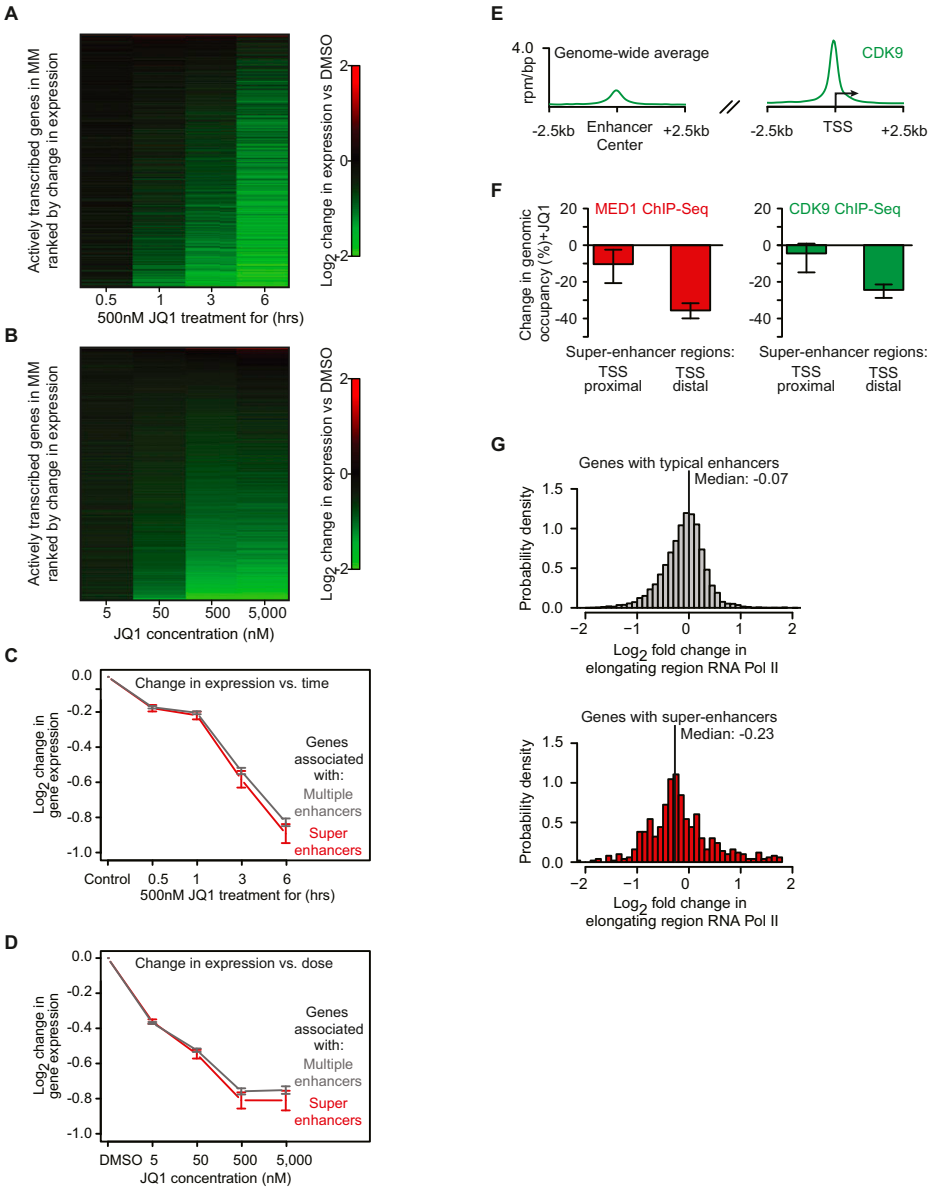

Figure S3. Transcription of Super-Enhancer-Associated Genes Is Highly Sensitive to BRD4 Inhibition, Related to Figure 6

(A and B) Heatmap of changes in gene expression for all actively transcribed genes after treatment with 500 nM JQ1 at various time points (A) or after treatment with various doses of JQ1 for 6 hr (B). Each line in the heatmap shows a single gene and is shaded relative to the change in gene expression compared to control untreated cells. Genes are ranked by average fold loss across the time course. The key on the right shows the relationship between color and change in gene expression with green indicative of loss of gene expression.

(C and D) Line graph showing the Log2 change in gene expression versus control cells after JQ1 treatment in a time- (C) or dose (D)-dependent manner for genes associated with multiple typical enhancers (gray line) or genes associated with super-enhancers (red line). The y axis shows the Log2 change in gene expression of JQ1 treated versus untreated control cells. The x axis shows time of 500 nM JQ1 treatment (C) or JQ1 treatment concentration at 6 hr (D). Error bars represent 95% confidence intervals of the mean (95% CI).

(E) Meta-gene representation of global CDK9 occupancy at enhancers and promoters. The x axis shows the ± 2.5kb region flanking either the center of enhancer regions (left) or the TSS of active genes. The y axis shows the average background subtracted ChIP-Seq signal in units of rpm/bp.

(F) Bar graphs showing the percentage loss of either MED1 (left, red) or CDK9 (right, green) at super-enhancer regions that are TSS proximal (left) or TSS distal (right). Error bars represent 95% confidence intervals of the mean (95% CI).

(G) Histograms showing the distribution of changes in RNA Pol II density in the elongating gene body region of genes for typical enhancer-associated genes (top, gray) or super-enhancer-associated genes (bottom, red). The median of the distribution is shown with a line. x axis shows the Log_2 change in RNA Pol II density in the elongating gene body region. y axis shows probability density of the distribution. The difference is distributions is significant by a Kolmogorov-Smirnov (KS) test (p value < 2e-16).

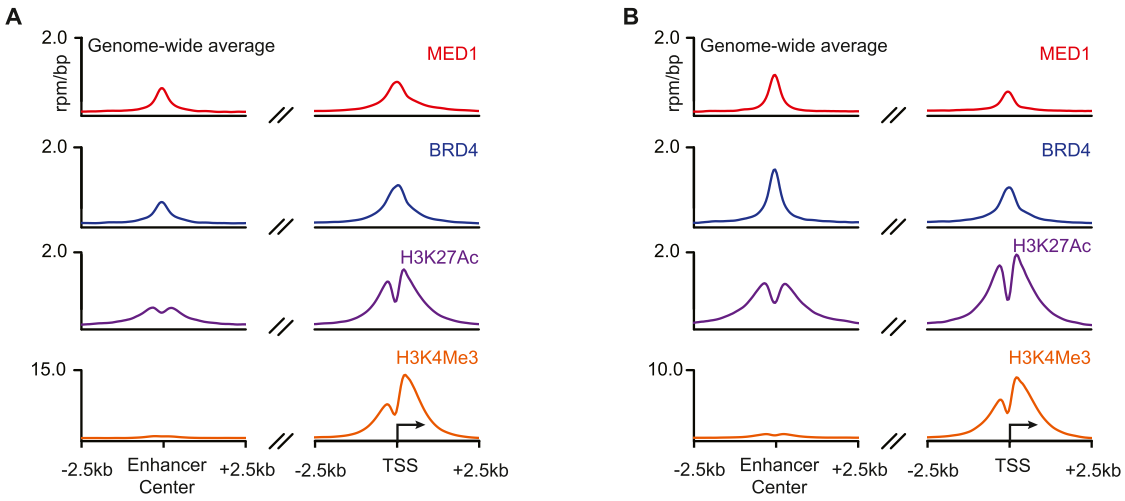

Figure S4. Super-Enhancers Are Associated with Key Genes in Other Cancers, Related to Figure 7

(A) Meta-gene representation of global MED1, BRD4, H3K27Ac, and H3K4Me3 occupancy at enhancers and promoters in the glioblastoma multiforme cell line U-87 MG. The x axis shows the ± 2.5kb region flanking either the center of enhancer regions (left) or the transcription start site (TSS) of active genes. The y axis shows the average background subtracted ChIP-Seq signal in units of rpm/bp.

(B) Meta-gene representation of global MED1, BRD4, H3K27Ac, and H3K4Me3 occupancy at enhancers and promoters in the small cell lung cancer cell line H2171. The x axis shows the ± 2.5kb region flanking either the center of enhancer regions (left) or the transcription start site (TSS) of active genes. The y axis shows the average background subtracted ChIP-Seq signal in units of rpm/bp.